

PRESIDENTIAL ADDRESS

Scales of disequilibrium and rates of equilibration during metamorphism\*

WILLIAM D. CARLSON†

Department of Geological Sciences, University of Texas at Austin, Austin, Texas 78712, U.S.A.

ABSTRACT

Mounting evidence suggests that partial disequilibrium—meaning disequilibrium for some elements, but not for others—may be a common but rarely detected phenomenon during metamorphic mineral growth, even in ordinary prograde reactions that progress to completion. Detailed examination of compositional variations in garnet crystals over a range of metamorphic grade suggests distinctly different scales of equilibration for common elements, with strong temperature dependence. Under lower greenschist-facies conditions, Fe and Mg may equilibrate at hand-sample scale, whereas Mn and Ca may not equilibrate even at millimeter-scale. Although Mn may achieve hand-sample-scale equilibration under upper greenschist-facies conditions, Ca and many trivalent cations (e.g., REEs) may not do so until temperatures exceed those of the middle amphibolite facies. Even in the lower granulite facies, some elements (e.g., Y, Yb) show indications of disequilibrium at sub-centimeter-scales during garnet growth.

Analysis and numerical modeling of undisputed disequilibrium textures demonstrate that the most common impediment to equilibration during metamorphism is the sluggishness of intergranular diffusion, the same mechanism known to govern porphyroblast crystallization in many metamorphic environments. Despite this importance to petrology, few quantitative determinations exist of intergranular diffusion rates under metamorphic conditions. Using numerical simulations of coupled intergranular and intracrystalline diffusion processes in coronal textures around partially resorbed garnet crystals from the Llano Uplift, U.S.A., a very precise and relatively accurate estimate is obtained for the rate of intergranular diffusion of Al in fluid-undersaturated systems. This result and an earlier estimate for fluid-saturated systems provide bracketing values for Al diffusivity during metamorphism.

INTRODUCTION

In a Presidential Address, the Society's outgoing president is granted by tradition the latitude to offer up thoughts, ruminations, even hunches—all with minimal review! I found this to be an irresistible opportunity to gather together a variety of intriguing recent observations on compositional anomalies in garnet that can be united by a set of somewhat unconventional interpretations, with provocative effect. From that exercise, described in Part I of this address, a pattern emerges that challenges one of metamorphic petrology's most closely held assumptions: several lines of reasoning point strongly toward the conclusion that even in the absence of textural indicators of incomplete reaction, common prograde metamorphic reactions may not achieve equilibrium for many elements at thin-section scale. Instead, different elements appear to equilibrate—or fail to equilibrate—over different geologically significant scales of time and length, because they are subject to substantially different rates of intergranular diffusion.

That inference adds to a growing recognition that the kinetics of intergranular diffusion govern rates of metamorphic crystallization and chemical equilibration in many ordinary circumstances. Unfortunately, those rates remain largely unknown. Part II of this address leaves speculation behind and presents a new approach that yields a high-precision, quantitative determination of the intergranular diffusivity of Al—the element that most studies have shown to control rates of recrystallization—by exploiting a natural example of coupled intergranular and intracrystalline diffusion.

PART I: SCALES OF DISEQUILIBRIUM

Disequilibrium is a familiar state of affairs in metamorphic rocks, but most of the commonly recognized examples of it are instances of incomplete reaction. Coronal microstructures around olivine crystals in metagabbros are exemplary cases of prograde reactions brought to a halt before they reached completion (e.g., Whitney and McLelland 1973; Ashworth and Birdi 1990; Johnson and Carlson 1990); similar textures surrounding resorbed garnets are equally persuasive cases of retrograde reactions that ceased before the reactants were wholly consumed (e.g., Misch and Onyeagocha 1976; Carlson and Johnson 1991). Somewhat more subtle and decidedly more complicated are linked segregations and pseudomorphous growth structures, like

\* Adapted from the Presidential Address given at the annual meeting of the Mineralogical Society of America, November 14, 2000, in Reno, Nevada.

† E-mail: wcarlson@mail.utexas.edu

those described elegantly by Carmichael (1969) and Foster (1986); again, these are systems that display, in obvious textural relationships, reactions arrested while still in progress. All of the foregoing examples have been explained in impressive detail by non-equilibrium thermodynamic models that have at their core the concept of intergranular diffusion as the rate-limiting mechanism during recrystallization.

Evidence is also accumulating, however, to demonstrate that intergranular diffusion is rate-limiting in many reactions that have gone to completion (Carlson 1989; Vance and O'Nions 1990; Carlson and Denison 1992; Carlson et al. 1995; Denison and Carlson 1997; Hirsch 2000; Hirsch and Carlson 2001). One wonders if these rocks might not have experienced significant levels of disequilibrium during mineral growth, just like their counterparts in which reactions terminated before completion, considering that their recrystallization was similarly governed by the kinetics of intergranular diffusion. The observations reviewed below suggest that many such rocks do indeed harbor evidence of a failure to equilibrate at thin-section scale during mineral growth, despite their lack of any indicators of incomplete reaction. In fact, certain anomalies of garnet composition in these rocks may constitute a record of systematic variations in the length scales over which different elements can equilibrate at different metamorphic grades.

### Background

The predominance of intergranular diffusion as a kinetic control on the crystallization of porphyroblasts can be detected in several ways, including assessment of normalized rates of radial growth as a function of crystal size (e.g., Kretz 1974; Carlson 1989), and comparison of absolute growth rates from isotopic chronometry with theoretical or measured rates for surface-reaction-controlled kinetics (e.g., Vance and O'Nions 1990, p. 237). But the methods with greatest relevance to the question of disequilibrium during mineral growth are those that are based on quantitative analysis of the sizes and locations of crystals in porphyroblastic textures. Nucleation-and-growth processes controlled by rates of intergranular diffusion generate spatial arrays of porphyroblasts with larger mean separations between nearest neighbors than would be found in a random array of the same crystal number density; these arrays also exhibit a correlation between crystal size and the degree of isolation of a crystal from its neighbors (Carlson 1989; Hirsch et al. 2000). Both effects arise because a local minimum in the chemical affinity for the reaction develops around each growing porphyroblast during crystallization, as it extracts nutrients from its immediate surroundings (Fig. 1). Close to the crystal, where the chemical affinity drops below the minimum value needed to overcome the energetic barrier to nucleation, a zone develops in which further nucleation is prohibited; this effect produces a tendency toward spatial ordering in the crystal array. When the zones from which nutrients have been partly depleted grow into convergence for two neighboring crystals, the growth rate for both declines in response to competition for the limited nutrient supply; this effect produces a correlation between crystal size and isolation. Gradients in chemical affinity must be supported by gradients in the chemical potential of one or more of the reacting species, and for this reason

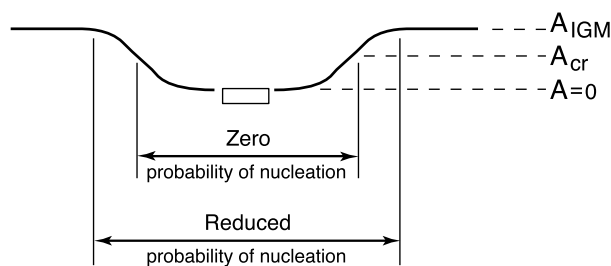


**FIGURE 1.** Schematic diagram of gradient in chemical affinity in the intergranular medium ( $A_{IGM}$ ) produced in reactions limited by rates of intergranular diffusion. At the center of the diagram is a growing porphyroblast, whose surface is presumed to be in local equilibrium with the IGM ( $A = 0$ ). In regions close to the crystal, where the reaction affinity is less than the critical value required for nucleation ( $A < A_{cr}$ ), nucleation is prohibited; in regions further away from the crystal, where intergranular diffusion has been effective in diminishing the reaction affinity, nucleation rates are reduced.

they have great significance: a gradient in chemical potential is, after all, the very definition of disequilibrium!

Evidence for reaction mechanisms governed by the kinetics of intergranular diffusion is becoming common, in the form of crystal arrays with spatial ordering and with significant size-isolation correlations. Documented examples, based on spatial data acquired by means of high-resolution X-ray computed tomography, appear in Carlson (1989), Denison and Carlson (1997), Hirsch (2000), and Hirsch and Carlson (2001). Combining these studies with other, unpublished results from our laboratory provides data for a total of 19 specimens. The data are mostly for garnet, but include two studies of porphyroblastic biotite. The specimens span a wide range of porphyroblast size and metamorphic conditions (greenschist through granulite facies, plus blueschist facies), and include mafic, pelitic, and calcareous bulk compositions. Although this data set is dominated by garnet in the middle-amphibolite facies, diffusion-controlled mechanisms are nearly universal within it: 16 of the 19 specimens exhibit statistically significant indicators of diffusion-controlled nucleation and growth. (The three other specimens were specifically selected to represent systems in which diffusion-controlled growth might not be expected to be the dominant mechanism: they included non-aluminous porphyroblasts of magnetite and diopside, and garnet crystallized in a reaction driven by infiltration of an aqueous fluid into a carbonate rock. Data from these specimens failed to negate the null hypothesis of a random spatial distribution, although this result might be due in part to the relatively low number of crystals available for analysis in the cases of garnet and magnetite, or to other complicating factors.)

Given this widespread occurrence of diffusion-controlled crystallization during metamorphism, the question immediately arises: which is the element whose diffusion is rate-limiting? Non-equilibrium models of layered coronal textures allow determination, in many cases, of relative rates of intergranular diffusion for different elements (e.g., Joesten 1977; Ashworth and Sheplev 1997). Aluminum repeatedly appears as the slow-

est to diffuse through the intergranular medium in modeling efforts that yield unambiguous measures of relative diffusion rates (see review by Ashworth and Sheplev 1997), so the kinetics of intergranular diffusion of Al is commonly viewed as the rate-limiting factor in the crystallization of layered coronas.

Although coronal textures commonly form in fluid-under-saturated circumstances, it is likely that Al is also the slowest-diffusing major component in fluid-saturated circumstances; in both cases, it is principally the low solubility of Al in the intergranular medium that accounts for its sluggish diffusional transport. One would therefore conclude that a chemical-potential difference for Al will be the predominant contributor to the chemical-affinity gradient around a growing aluminous porphyroblast. But it is an oversimplification to regard the chemical-affinity gradient merely as the reflection of a gradient in chemical potential for a single element. The relationship between the gradient in chemical affinity and multiple individual gradients in chemical potential can be complex. If all elements diffuse at approximately the same rate, then the chemical-potential gradients for all species will be significant components of the chemical-affinity gradient. If, however, one or more of the elements diffuses much more rapidly than the slowest-diffusing element, then the more rapidly transported species will have shallower gradients; in the limit, the chemical-potential gradient for very rapidly transported species will go to zero. Because rapid diffusion may thus flatten the intergranular chemical potential gradients for some elements, while slow diffusion for others preserves steep or intermediate gradients, then for any chosen length scale and time scale, some elements may have equilibrated while others may not (Fig. 2). Such a situation can be termed "partial equilibrium:" equilibrium with respect to some, but not all, reactive components.

The implications of partial disequilibrium between a growing porphyroblast and distal portions of its precursor matrix are self-evident but profound. Efforts at geothermobarometry, assessment of phase equilibria, and construction of  $P$ - $T$ - $t$  paths based on compositional variations in minerals depend on the assumption that minerals equilibrate with one another during growth, over length scales measured by the separation among reactant crystals. Conditions during mineral growth will be re-

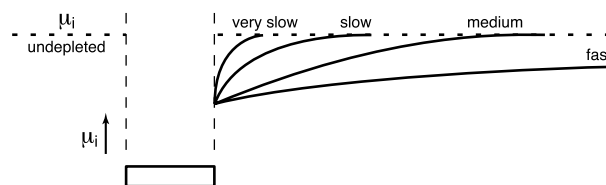


**FIGURE 2.** Schematic chemical-potential gradients around a growing porphyroblast for elements with very slow, slow, medium, and fast rates of inter-granular diffusion. Only if rates of intergranular diffusion are rapid enough to flatten chemical-potential gradients will equilibrium concentrations of an element be incorporated into the growing crystal.

corded accurately only in those chemical systems based on elements that diffuse through the intergranular medium rapidly enough to eliminate intergranular gradients in their chemical potentials.

But is there any evidence in nature of significant disequilibrium during mineral growth for elements important to petrologic inferences? I believe there is. The repository for that evidence is compositional variation in garnet, a mineral with a remarkable ability to incorporate in its major- and trace-element concentrations a wealth of detail about the chemistry of its surroundings and the physical conditions under which it grew. Some recent observations of compositional anomalies in garnet are collected below, and interpreted as records of partial disequilibrium during metamorphism—the expression of a set of relative rates of intergranular diffusion that changes in systematic ways with increasing metamorphic grade.

### Observations

The observations pertinent to detection of partial disequilibrium are organized below in order of increasing metamorphic grade, which places the most controversial interpretations at the beginning and end of the story.

**Greenschist Facies.** Specimens from the garnet zone at Harpswell Neck, Maine (Lang and Dunn 1990) have been recently studied by Daniel and Spear (1998, 1999), Spear and Daniel (1998, 2001), and Hirsch (2000). X-ray maps of the distribution of Mn on central sections show patchy distributions with multiple separate maxima in the interiors of crystals, some in the shape of microfolds or crenulations. Although Fe and Mg show similarly patchy distributions (antithetic to Mn) in the interiors of crystals, Ca distributions tend to be concentric about the morphological center of the crystal. Importantly, all crystals have nearly identical concentrations of Mn, Fe, and Mg at their rims, and these peripheral regions lack the patchiness and local Mn maxima found in the interiors of the crystals.

The fact that compositional contours for different elements cut across one another is immediate evidence that not all of them could have been simultaneously in equilibrium during the periods of garnet growth represented by the interior portions of the crystal. Spear and Daniel (2001, p. 184) conclude from their analysis that "Mn, Fe, and Mg are in equilibrium throughout the thin section, whereas Ca is transport-limited" (and therefore not in equilibrium at scales larger than that of each individual porphyroblast). For Ca, this result corroborates earlier similar findings by Chernoff and Carlson (1997) in different rocks at higher grade, described in the following section.

Isolated regions of high Mn in these X-ray maps present a greater problem of interpretation. Originally, these regions were claimed to be separate sites of nucleation that grew and coalesced into a single crystal (Spear and Daniel 1998), but subsequent studies (Daniel et al. 1999; Hirsch 2000) have shown that all parts of each garnet share a mutual crystallographic orientation (within about  $\pm 1^\circ$ ). Spear and Daniel (2001), noting that some Mn maxima had the shapes of crenulation folds, then argued that early formed crystals took on the shape of these folds, so that in their words (p. 183), the paradox is "re-

solved by recognition that the isolated high-Mn zones are connected in the third dimension in the crenulation fold.” However, this conclusion is difficult to reconcile with the earlier statement made in Spear and Daniel (1998, p. 7) that “examination of selected garnet crystals in 3-dimensions ... indicates that most of the nuclei are not connected in the third dimension” and with the later inability of Spear and Yao (2001) to identify, in a higher resolution study, connections among isolated high-Mn regions; they wrote: “islands of garnet must ... be connected to the garnet mainland by channels too small to image (image resolution =  $1 \times 1 \times 4 \mu\text{m}$ ).”

An alternative interpretation of these observations is presented by Hirsch (2000). If one abandons the supposition that Mn is in equilibrium throughout the thin section, at least during the earliest stages of garnet growth, then the observations can be reconciled to a model of roughly concentric growth of a garnet from its morphological center, with the crystal incorporating pre-existing heterogeneities in Mn-content of the precursor matrix as it overgrows them (Fig. 3). This is a form of compositional variation called “overprint zoning” by Yang and Rivers (2001) in the occurrence described below. It requires very limited scales of intergranular diffusion for Mn during the lowest-temperature part of the garnet growth history, and implies that Fe and Mg concentrations are locally influenced by Mn concentrations that vary significantly from place to place on the surface of the growing garnet.

It is noteworthy that these are very manganiferous rocks, with maximum Mn contents in garnet of about 50 mol% spessartine—so crystallization in garnet cores may have begun at comparatively very low temperatures. As temperatures rose, rates of intergranular diffusion would have increased exponentially, providing a ready explanation for the observations that the outermost portions of the crystals do not contain local Mn maxima, and that the rim compositions of all crystals are equivalent throughout the thin section.

Thus I favor the possibly unconventional interpretation that

Hirsch (2000) places on these observations, namely that the Harpswell Neck garnets have captured a transitional regime for diffusional transport of Mn. During early, low-temperature growth, intergranular diffusion of Mn was restricted to scales on the order of the size of the precursor matrix grains; with exponential thermal acceleration, this length scale expanded during the interval of garnet growth to permit equilibration at thin-section scale by the time garnet crystallization ceased.

**Middle Amphibolite Facies.** One of the first studies to document the failure of Ca to equilibrate at thin-section scale during garnet growth was that of Chernoff and Carlson (1997). In that study of garnet zoning patterns in middle amphibolite facies pelitic rocks in the Picuris Range of north-central New Mexico, concentrations of Fe, Mn, and Mg displayed smooth, radially symmetrical zoning, and their compositions were found to correlate strongly with one another. Calcium concentrations, however, were found to be uncorrelated, and to exhibit sharp spikes roughly halfway between core and rim in crystals of all sizes (Fig. 4). Using central Mn content (with centers located by X-ray computed tomography) as a proxy for nucleation time, and the Mn concentration at the Ca spike as a proxy for the timing of spike generation (see justifications in Chernoff and Carlson 1997, p. 430), a striking correlation was found between the two: the earlier a crystal nucleates, the earlier it crystallizes a Ca spike. As explained by Chernoff and Carlson (1997, p. 431), the Ca spikes therefore cannot be event markers (features marking a change in intensive parameters that affected all crystals in the rock simultaneously), but must instead be generated by factors related to the local extent of reaction, that is, within the local diffusional domain of each porphyroblast. Calcium cannot have been in rock-wide equilibrium during garnet growth.

Subsequent analysis of trace-element distributions (e.g., P, Y, Ti, Yb, Sc) with the electron microprobe showed marked perturbations that coincided exactly with the Ca spikes (Fig. 4); so too did SIMS analyses for Y, Zr, Hf, Li, Na, and Sr (see

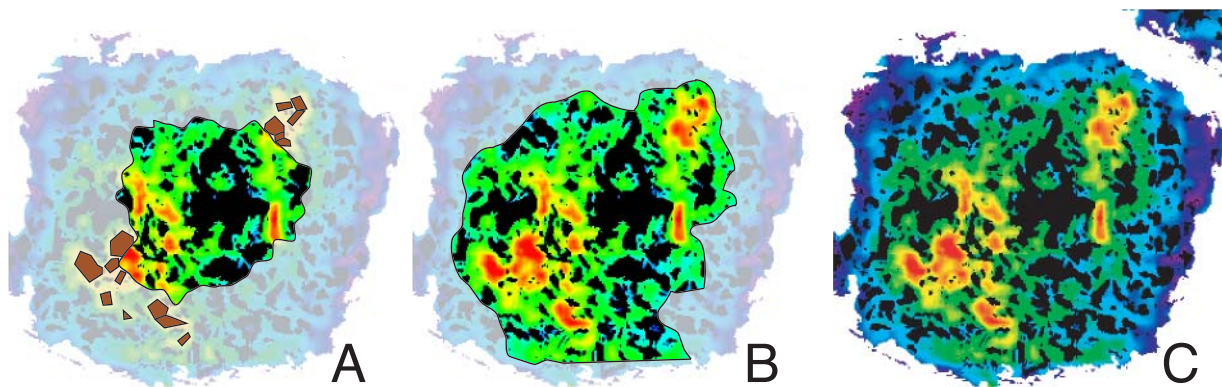


**FIGURE 3.** Compositional variation for Mn in Harpswell Neck garnet, with interpretation following Hirsch (2000). Part A shows an early stage in the garnet growth (light-colored regions are portions of the garnet not yet crystallized at this stage). With further growth, as indicated in part B, Mn-rich heterogeneities in the precursor matrix (perhaps sourced by chlorite or ilmenite crystals, shown in brown in part A) are overgrown and incorporated into the garnet, because rates of intergranular diffusion for Mn are too slow to allow for its equilibrium distribution at length scales larger than that of the grain size of the precursor. Near the end of growth, as shown in part C, rising temperature has increased the scale of intergranular diffusion of Mn so that outer portions of the crystal lack the patchy character of the interior; rim compositions are constant around the edge of each crystal and uniform from crystal to crystal. (From Hirsch 2000.)

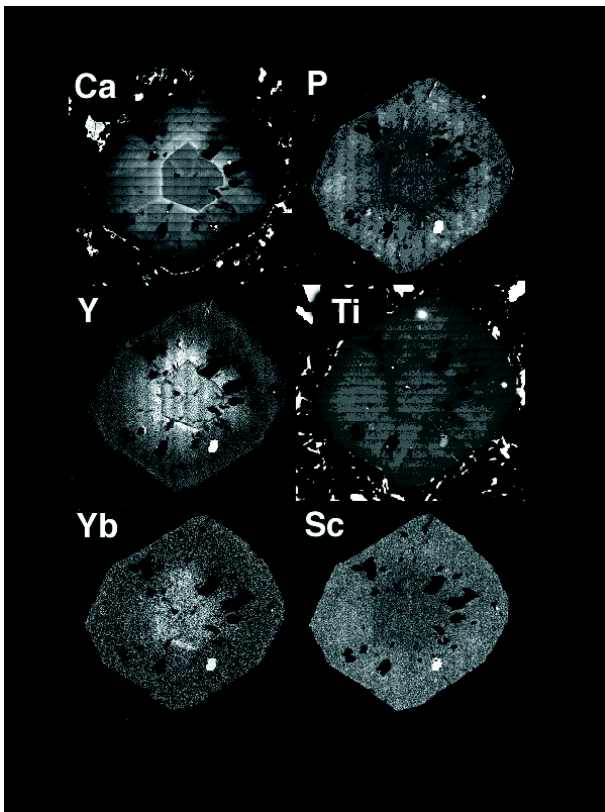


**FIGURE 4.** X-ray maps for central section through a garnet crystal 1 mm in diameter from the Picuris Range. The strikingly euhedral spike in Ca (*top left*) correlates exactly in position with abrupt modulations of concentrations of Y, Yb, P, Ti, and Sc. Locations of these features correlate strongly with crystal size, and cannot be reconciled to any hypothesis for their simultaneous origin in different crystals as part of a rock-wide fluctuation in any intensive parameter. Instead, these compositional variations are evidence of a failure of these elements to equilibrate at scales larger than the mean separation between crystals. [Modified from Chernoff and Carlson (1999).]

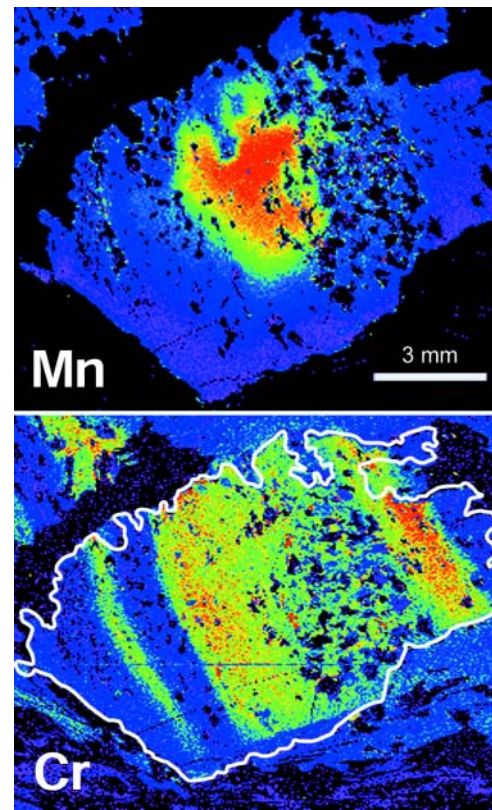


**FIGURE 5.** “Overprint zoning” illustrated by contrast in X-ray maps between distributions of Mn (*top*) and Cr (*bottom*) in a garnet crystal from western Labrador. Banding in Cr is parallel to a planar fabric of inclusions. Whereas the concentric Mn zoning is consistent with growth from a fully equilibrated, progressively depleted matrix, the Cr zoning is clearly inherited from original heterogeneities in the precursor. [Modified from Yang and Rivers (2001).]

Figs. 1 and 2 in Chernoff and Carlson 1999). One is forced to accept that the concentrations of all of these elements in the Picuris garnets were determined not by rock-wide equilibration with matrix phases, but by local factors, probably discontinuous changes in the minor phases participating in the garnet-forming reaction (Chernoff and Carlson 1999, p. 556).

**Upper Amphibolite Facies.** Some of the most extraordinary and clear-cut examples of disequilibrium during garnet growth are presented by Yang and Rivers (2001). For example, in a large crystal from a “migmatite zone” (upper amphibolite facies) in the Grenville Province of western Labrador, concentric Mn zoning contrasts markedly with a distinct banding of Cr-rich and Cr-poor layers, parallel to an included fabric (Fig. 5). Their conclusion (p. 468) seems inescapable: “...Cr zoning in the garnet[s] ...appears to have been inherited from the Cr

distribution present in the pre-existing fabric ( $S_1$ ) that was overprinted during garnet growth.”

**Granulite Facies.** Garnets crystallizing in metamorphic events culminating in the granulite facies are typically partially or wholly homogenized by intracrystalline (volume) diffusion—at least with respect to major elements—thereby destroying for those elements the record of compositional variation in garnet available in lower-grade rocks. Nevertheless, it is reasonable to infer that at temperatures sufficient to redistribute major elements at the scale of several millimeters by intracrystalline diffusion, external transport by diffusion through an intergranular fluid would be rapid enough to equilibrate those elements at thin-section scale in the matrix. But what about other species?

A delicate indication that Y and Yb fail to equilibrate rock-

wide even at granulite-facies conditions comes from the reconnaissance study of Barnes and Carlson (2001) on rocks from the western Llano Uplift of central Texas that reached peak metamorphic temperatures of about 750 °C (Wilkerson et al. 1988; Anderson 2001). X-ray maps of Y and Yb were made on central sections through three crystals of markedly different size from the same 3 cm tall section of a 2.5 cm diameter core (central sections were located by X-ray computed tomography). Although the maps for the largest garnet and the smallest garnet were featureless, the map of the intermediate-sized garnet shows a clearly discernible euhedral ring for Y (Fig. 6) and a fainter euhedral ring at the same location for Yb. The resemblance to the Ca spikes in the Picuris Range rocks is striking, but the Y distribution must have a somewhat different origin, insofar as it was seen in only one of the three nearby crystals. Even so, it tells much the same story: the Y enrichment cannot be a rock-wide event marker, because it does not appear in the larger crystal imaged from the same thin section. Instead, some local source of Y and Yb must have become active midway through the growth of the intermediate-sized garnet, providing Y and Yb to the surface of this crystal, but not affecting coexisting crystals nearby. Given this interpretation, one must conclude that even under granulite-facies conditions, intergranular diffusion of Y and Yb is too restricted to permit equilibration at thin-section scale.

### Discussion

My interpretation of the above observations is summarized in Figure 7. The evidence points to intergranular diffusion of Fe and Mg at rates sufficient to produce centimeter-scale equilibration over metamorphic time scales, even at the lowest temperatures of metamorphism. The Harpswell Neck data suggest

that Mn makes the transition from relatively sluggish to relatively rapid intergranular diffusion somewhere between the lower and upper greenschist facies. In both the Harpswell Neck rocks and those of the Picuris Range, we find evidence that Ca fails to equilibrate at centimeter-scale by intergranular diffusion at temperatures below those of the upper amphibolite facies. The Picuris data, the western Labrador study, and the tidbit of data from the Llano Uplift are consistent with the notion that trivalent, quadrivalent, and pentavalent cations do not equilibrate at centimeter-scale in the amphibolite facies, and probably do not do so even under lower granulite-facies conditions.

Obviously, there is a need for many more observations to put flesh on this skeletal hypothesis, and one purpose in presenting it in this forum is to stimulate further efforts toward that end. The critical question, of course, is whether these observations constitute a general pattern, or are merely a coincidental set of isolated occurrences. If the results are general, then it would appear that sluggish intergranular diffusion makes chemical disequilibrium commonplace during metamorphism.

As further data accumulate, it would be prudent to keep in mind that rates of intergranular diffusion depend on a number of factors other than just temperature—important ones are those that affect the bulk solubility of elements in the intergranular medium, such as the degree of fluid saturation or undersaturation; the abundance and connectivity of grain-edges to serve as diffusion pathways (which may be affected by deformational strain in the matrix during crystallization); and for some elements, perhaps, the chlorinity and oxygen fugacity of an aqueous fluid, if present. So against the general backdrop painted by Figure 7, one should expect to see substantial variations depending on the particular metamorphic environment.

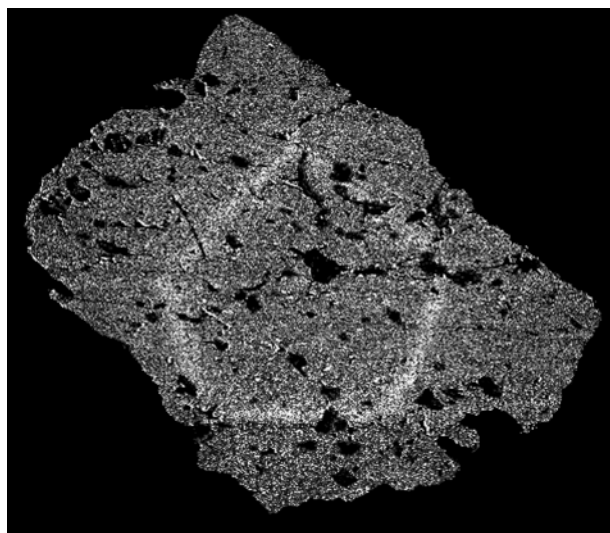


**FIGURE 6.** X-ray map of Y distribution in garnet from the Llano Uplift, which grew at peak temperatures of ~750 °C; brighter regions represent higher concentrations. The euhedral ring of high Y (and Yb) concentration, absent in nearby crystals, can be explained by invoking a local source of Y and Yb that was prevented from affecting nearby crystals by the sluggishness of intergranular diffusion of these elements.

### Equilibration at cm-scale over geologic time

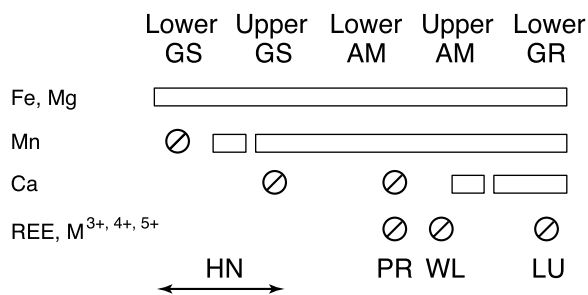


**FIGURE 7.** Summary of inferred equilibration behavior for various elements as a function of metamorphic grade. Bars represent conditions for which equilibration at centimeter-scale over geologic times is expected; circles with slashes represent circumstances for which evidence cited in the text makes such equilibration unlikely. GS = greenschist, AM = amphibolite, GR = granulite, HN = Harpswell Neck, PR = Picuris Range, WL = western Labrador, LU = Llano Uplift.

## PART II: RATES OF EQUILIBRATION

Whether or not the above generalizations are viable, the foregoing observations are a clear demonstration that rates of intergranular diffusion are vitally important determinants of the ability of rocks to maintain internal chemical equilibrium as they recrystallize. For that reason, those rates place inherent limitations on the ability of metamorphic rocks to record their geologic history. Accurate determination of those rates should therefore be a high priority among petrologists.

Unfortunately, relatively little is known about absolute rates of intergranular diffusion in nature. Laboratory determinations have proven extremely difficult (e.g., Brady 1983), and it is only recently, with the advent of the elegant experimental approach of Farver and Yund (1995a; 1995b; 1996; 2000a; 2000b), that reliable data have begun to emerge. And of course the applicability of those data to natural occurrences will remain suspect until confirmation can be found in the rocks themselves.

Faced with a paucity of experimental data, several investigators have attempted to extract constraints on rates of intergranular diffusion from natural occurrences (Vance and O'Nions 1990; Ashworth 1993; Carlson et al. 1995). These attempts have been frustrated, however, by relatively large uncertainties, principally due to difficulty in constraining tightly enough the time elapsed during events in which intergranular diffusion took place. What follows next is an analysis of unusual textures that exhibit clear coupling between intergranular diffusion and intracrystalline diffusion (the latter in garnet). Because rates of intracrystalline diffusion in garnet are reasonably well-known from experimental work at high temperatures, reliable time estimates can be obtained for the duration of the intergranular-diffusion event, leading to highly precise and reasonably accurate determinations of rates of intergranular diffusion.

### Overview of approach

Partially resorbed garnets in mafic rocks of the Llano Uplift in central Texas, U.S.A., are surrounded by layered coronal reaction textures and exhibit stranded intracrystalline diffusion profiles at their rims (Fig. 8). The strong spatial organization of layered coronal textures reflects their origin in reactions whose kinetics are governed by rates of intergranular diffusion between reactants across a growing product zone (Fisher 1977, p. 383); a recent review of the evidence for this conclusion may be found in Ashworth and Sheplev (1997). The complex evolution of the Llano coronas in particular has been successfully replicated by non-steady-state, open-system, local-equilibrium models of intergranular diffusion (Carlson and Johnson 1991). Modification of compositions at the rim of a garnet undergoing resorption has long been attributed to intracrystalline diffusion in response to partial re-equilibration of the periphery of the garnet with its surroundings, in numerous studies tracing back to that of de Béthune et al. (1975). Because the development of stranded intracrystalline diffusion profiles in relict Llano garnets is therefore intimately coupled to the resorption reaction, one can use laboratory determinations of intracrystalline diffusion rates in combination with quantitative analysis of the coronal textures to constrain rates of intergranular diffusion in nature.

Figure 9 illustrates the central concept. The steepness of

internal compositional profiles depends upon the relative rates of the resorption reaction and the intracrystalline diffusion that results from it. If resorption is rapid in comparison to rates of intracrystalline diffusion, then elements preferentially partitioned into the relict garnet tend to build up near the rim, and compositional perturbations at the rim are not communicated into the interior of the crystal, producing steep profiles restricted to the periphery of the relict garnet (Fig. 9a). But if intracrystalline diffusion can nearly keep pace with the resorption reaction, then elements preferentially partitioned into the relict garnet are rapidly transported inward down the concentration gradient, and the effects of resorption penetrate more deeply into the interior of the crystal, producing shallow profiles (Fig. 9b). For elements that are preferentially partitioned into the reaction products, the same reasoning applies, but concentrations near the rim of the garnet decrease outward.

In this work, the relative rates of these processes in the Llano rocks are assessed using a numerical simulation of multi-component intracrystalline diffusion that computes the compositional changes for Fe, Mg, Mn, and Ca resulting from resorption. Reaction rates are quantified by establishing values for the input parameters of the model that produce congruence between observed zoning profiles and those predicted by the model. The input parameters are sufficiently well-constrained that all but one of them can be considered as known and treated as fixed; thus the fitting procedure involves only a single unknown parameter. The numerical simulation yields estimates for the duration of the resorption reaction in each corona studied, providing a critical (and surprisingly precise) time constraint. The duration of the resorption event computed in this way is then used in conjunction with measured widths of coronal reaction zones to determine rates of intergranular diffusion.

### Specimens and their geologic setting

The coronal reaction textures central to this study are a consequence of the two-stage metamorphic history of the Llano Uplift (Carlson 1998; Mosher 1998), in which original regional metamorphism resulting from Mesoproterozoic collisional orogeny along the southern margin of Laurentia was subsequently overprinted by recrystallization accompanying widespread intrusion of granitic plutons. In the earlier regional event, garnet crystallized in mafic rocks under conditions transitional among the amphibolite, granulite, and eclogite facies; later recrystallization took place at lower pressures that rendered garnet unstable, and under largely static conditions that allowed development and preservation of coronal reaction zones.

Peak temperatures and pressures during regional metamorphism—preserved only in scattered localities—show geographic variation at present levels of exposure (Carlson 1998). This fact was exploited in the present study by choosing specimens from occurrences in the western portion of the uplift, where peak temperatures during garnet crystallization reached ~750 °C, sufficient to nearly homogenize original growth-zoning profiles in all but the largest garnets (Carlson and Schwarze 1997). Field relationships for these rocks, together with detailed petrologic and petrographic information, are provided by Wilkerson et al. (1988) and Anderson (2001).

Although resorption is evident for almandine-rich garnets in all bulk compositions, the emphasis in this study is on reactions between garnet and sodic clinopyroxene in mafic rocks, because the mineralogical features of those coronas provide unequivocal evidence for the original radii of the garnet crystals and for the extent of reaction in the matrix surrounding the original garnet, two quantities vital to accurate modeling. In contrast, garnets in pelitic and semi-pelitic rocks—although evincing resorption in the form of stranded diffusion profiles—are commonly surrounded by a coarse-grained quartzofelds-

pathic matrix that generally lacks features to demarcate clearly the original extent of the garnet and the portion of the matrix involved in the garnet-resorption reaction.

As described in Wilkerson et al. (1988) and Anderson (2001), the coronas in mafic rocks from the western portion of the uplift are a close match, texturally and mineralogically, to those from the northern part of the uplift that have been analyzed in detail by Carlson and Johnson (1991). Two quantities essential to the numerical simulations must be measured in the coronal textures: the original radius of the garnet crystal, and the total

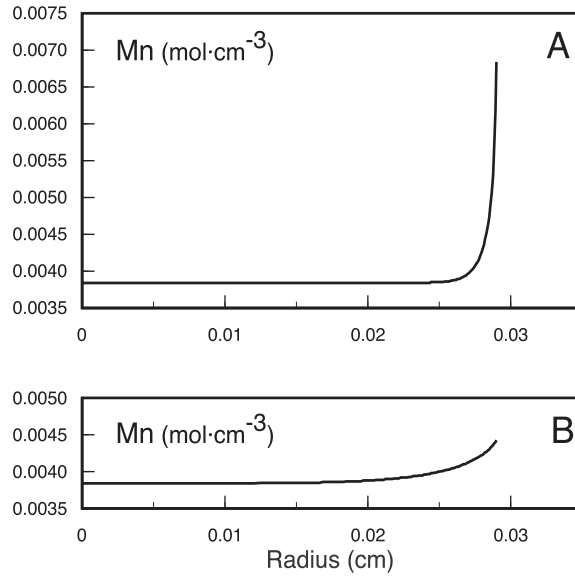
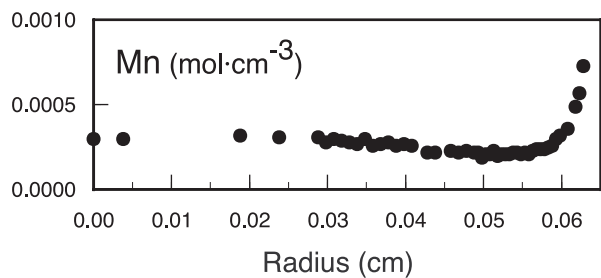
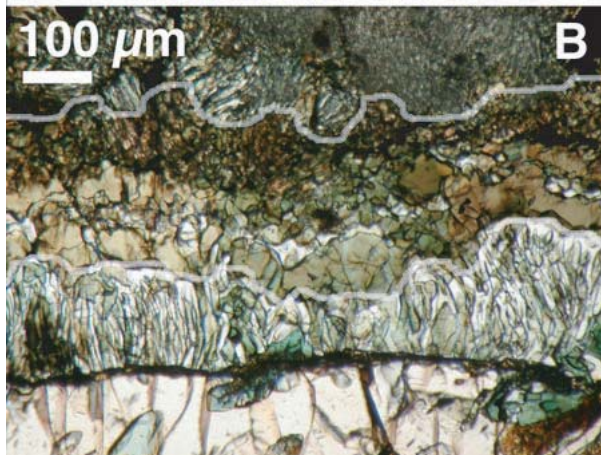
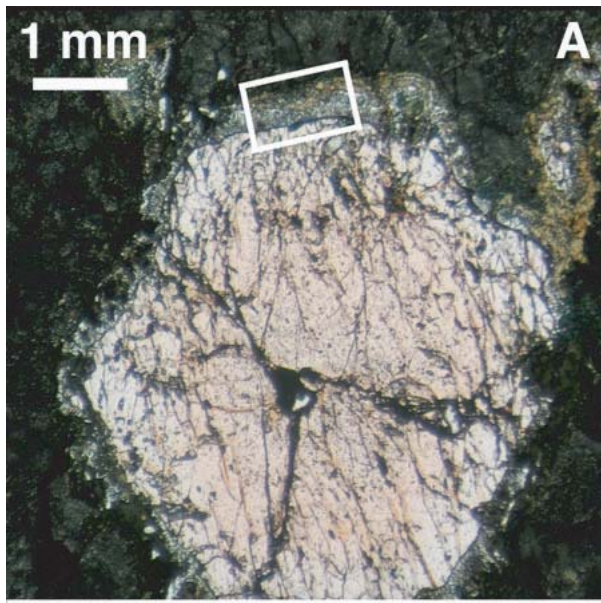


**FIGURE 9.** Comparison of stranded diffusion profiles produced by different *relative* rates of resorption and intracrystalline diffusion. Ratio between rate of resorption and rate of intracrystalline diffusion is greater in part A than in part B by a factor of 8.5; all other conditions and features, including total amount of Mn in relict crystal, are identical.

**FIGURE 8.** (A) Photomicrograph in polarized light (uncrossed polars) of large garnet crystal in thin section of specimen PH-12a from the western Llano Uplift, showing reaction rim separating it from the surrounding matrix. White box outlines area enlarged in part B. (B) Photomicrograph in polarized light (uncrossed polars) of layered coronal reaction zone. Relict garnet is at bottom of photo. Next layer upward is a symplectite of white plagioclase and green amphibole; its upper limit, marked on image by faint line, is the inferred location of the original boundary between reactants. Above that boundary is a layer composed predominantly of green amphibole, with a narrow band of white plagioclase near its center; this borders on a brownish zone that comprises a symplectite of plagioclase, amphibole, and orthopyroxene. The upper faint line marks the boundary with a top zone of intergrown plagioclase and sodian augite, secondary after original omphacitic clinopyroxene. Diagram at bottom of figure shows a stranded intracrystalline diffusion profile for Mn in a different, much smaller garnet crystal from the same locality.

width of the diffusional reaction zone when reaction ceased. The non-equilibrium thermodynamic models of Carlson and Johnson (1991) demonstrate that the original extent of the central garnet is closely approximated by the outer limit of the zone of symplectitic amphibole + plagioclase, with magnetite commonly distributed around its periphery; this limit is shown by the lower boundary drawn in Figure 8. The total width of the reaction zone spans the distance from the outer rim of the relict garnet crystal to the interface between the layer of intergrown orthopyroxene + amphibole + plagioclase and the symplectite of sodian augite + oligoclase (which replaced the omphacitic clinopyroxene originally present in equilibrium with garnet); this interface is shown by the upper boundary drawn in Figure 8. In many cases this latter boundary is difficult to locate by optical microscopy, but both boundaries are quite evident in backscattered-electron (BSE) images; Figure 6 of Carlson and Johnson (1991) provides examples.

Restricted access of hydrous components is evidently required to produce these coronas. Where fluids were likely to have been abundant, resorption of garnet is enhanced or complete, as at the margins of large metamafic bodies (Jordan 1970, p. 13) or small ones (Zumbro 1999, p. 305, 307), or in the vicinity of late shear zones (Davidow 1996, p. 48) or pegmatite dikes (Carlson and Johnson 1991, p. 758). Only in the interiors of undisturbed bodies are relict garnets common. Where garnet relics are preserved, the extent of resorption may vary from incipient to nearly complete over scales of only a few meters in the field, an observation again consistent with local differences in the ease of access of hydrous components to the sites of reaction. Overall, the requirement for preservation of garnet relics appears to be conditions like those described by Ashworth (1993, p. 331); in explaining the origin of similar coronal textures, he concluded that hydrous components were ubiquitously available for reaction at grain boundaries, but probably not present as a separate fluid phase. The development of symplectitic layers in the coronas from most Llano localities, including those of this study, can be taken as further evidence for recrystallization in the absence of a separate fluid phase: Ashworth and Chambers (2000, p. 302) argue that in the presence of a fluid phase, symplectitic reaction mechanisms are much less likely than other mechanisms that lead instead to granular textures.

Hydrous components appear to have been present throughout the cooling history of the rocks, however, so the failure of the reaction to reach completion was caused by the exponential deceleration of reaction kinetics as temperature dropped, and was *not* the result of a limited supply of H<sub>2</sub>O that prevented further formation of hydrous products. The most direct evidence in support of this inference is that there is no petrographic indication of a reduction in H<sub>2</sub>O activity during the final stages of coronal development, even though the coronal layers record in great detail their evolution in response to changes in the local abundance of other reactants (cf., Fig. 6 and discussion on p. 770–771 of Carlson and Johnson 1991). It is therefore concluded that hydrous components were present throughout the reaction history, and that resorption continued during cooling until rates of transport by intergranular diffusion declined to levels insufficient to sustain appreciable reaction. Consistent

with this inference is the observation, documented in Carlson and Johnson (1991, in their Figs. 3 and 4), that where garnet was originally in contact with quartz, coronas formed that contain only anhydrous products (pyroxene and plagioclase), but these are equivalent in width to coronas elsewhere with hydrous products (amphibole).

Rates of intracrystalline diffusion in garnet vary with composition. Core and rim analyses for major elements in the fourteen compositional traverses made in this study appear in Table 1, and Figure 10 presents a comparison between the collection of core and rim compositions of garnets in this study and the near-end-member compositions used in relevant intracrystalline diffusion experiments by Chakraborty and Ganguly (1992). The Llano garnets carry substantially more Mg and Ca than the experimental crystals, a factor that complicates selection of appropriate values for rates of intracrystalline diffusion.

### Methods

Accurate measurements of zoning profiles, original garnet radii, and coronal widths depend critically upon obtaining central sections through the coronal reaction zones and the relict garnet crystals at their centers. To this end, specimens that appeared promising after thin-section examination were imaged using high-resolution X-ray computed tomography (Carlson and Denison 1992; Ketchum and Carlson 2001), which allowed selection of near-spherical garnets displaying a wide range of sizes and degrees of resorption, and which provided precise information on crystal sizes and locations.

Using the tomographic data as a guide, specimens were carefully ground to expose sections precisely through the morphological centers of garnet crystals. Polished surfaces were then photographed in reflected light and imaged with backscattered electrons. From these images, measurements were made of the radii of relict garnet crystals, the widths of the plagioclase-rich coronal layers (to determine the original garnet radii), and the total widths of the reaction-product zone.

X-ray maps were produced on the electron microprobe to examine the distribution of major elements on central sections through garnet crystals, and these maps were used to identify optimal locations of core-to-rim traverses for analysis of major-element compositional profiles. Quantitative wavelength-dispersive analyses along the chosen lines of traverse were made on a JEOL 733 Superprobe. Data reduction employed well-characterized natural and synthetic standards. To define clearly the shapes of the stranded intracrystalline diffusion profiles, a minimum beam diameter (nominally ~1 μm) was used, and the spacing between analysis points was chosen to be 5 μm in the region of diffusively modified compositions near the rim of the relict garnet, but 10–20 μm or larger in the central, unaffected regions. Typical analytical conditions were 15 or 20 kV accelerating voltage and 30–75 nA sample current on brass, with 20–30 s counting times.

### Numerical simulation of coupled intergranular and intracrystalline diffusion

Quantitative estimates of the duration of the resorption reactions, which lead to constraints on intergranular diffusivities, were extracted from natural coronal textures by numerical simu-

TABLE 1. Garnet compositions

	LU93-22a		LU93-22a'		LU93-22b		LU93-22b'		LU93-26b		LU93-26b'		LU93-26c	
	Core	Rim	Core	Rim	Core	Rim	Core	Rim	Core	Rim	Core	Rim	Core	Rim
MgO	4.43	4.24	4.48	3.77	3.02	3.87	3.03	3.46	5.44	4.79	5.44	4.84	6.29	4.72
CaO	11.77	11.17	11.84	11.05	11.77	8.26	11.71	9.25	8.77	8.61	8.77	7.28	8.21	7.14
MnO	0.91	1.10	0.87	1.32	1.08	1.78	1.05	1.65	0.61	1.03	0.61	1.22	0.55	1.33
FeO	23.06	22.91	22.99	24.16	24.87	27.14	25.01	25.17	25.03	24.96	25.03	26.99	24.38	27.16
Al <sub>2</sub> O <sub>3</sub>	21.81	21.63	21.90	21.38	21.08	21.05	21.10	21.32	21.79	21.43	21.79	21.77	21.52	21.30
SiO <sub>2</sub>	39.07	38.40	39.11	38.81	38.55	38.89	38.30	39.62	39.16	38.55	39.16	38.78	39.23	38.93
Total	101.05	99.45	101.19	100.49	100.36	100.99	100.20	100.44	100.79	99.37	100.79	100.89	100.18	100.57
X <sub>alm</sub>	0.491	0.499	0.489	0.521	0.536	0.585	0.538	0.561	0.537	0.548	0.537	0.584	0.522	0.590
X <sub>grs</sub>	0.321	0.312	0.323	0.305	0.325	0.228	0.323	0.264	0.241	0.242	0.241	0.202	0.225	0.199
X <sub>pyp</sub>	0.168	0.165	0.170	0.145	0.116	0.149	0.116	0.137	0.208	0.187	0.208	0.187	0.240	0.182
X <sub>sps</sub>	0.020	0.024	0.019	0.029	0.024	0.039	0.023	0.037	0.013	0.023	0.013	0.027	0.012	0.029

\* Analysis in weight percent; total Fe as FeO.

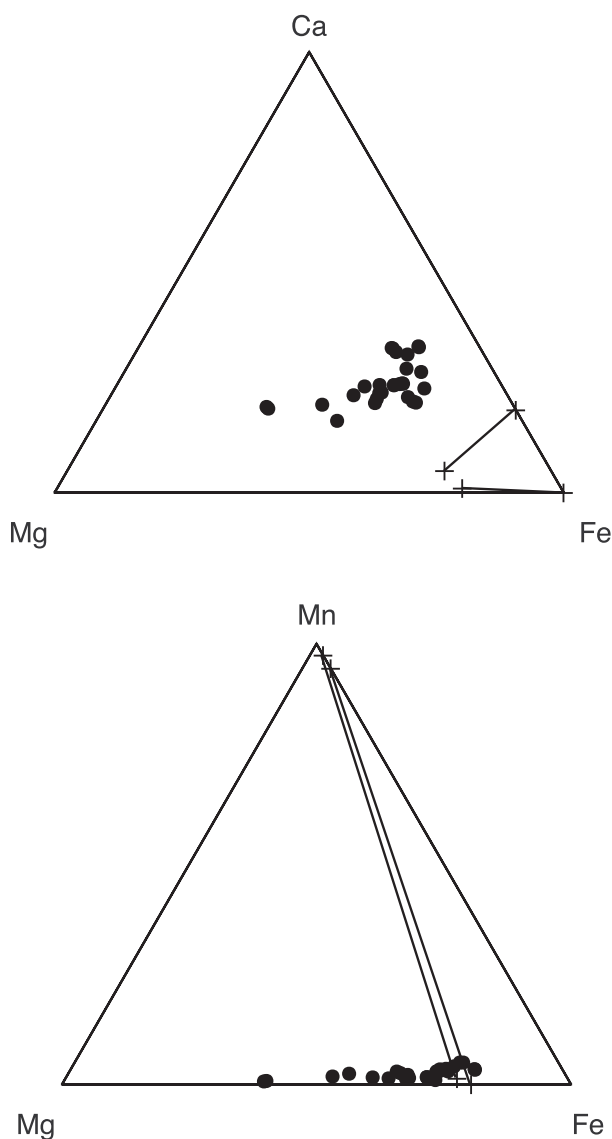


FIGURE 10. Garnet compositions (mole percent) in the ternary systems Ca-Mg-Fe and Mn-Mg-Fe. Dots represent the collection of core and rim analyses in Table 1; crosses linked by lines represent the pairs of compositions used in the intracrystalline diffusion experiments of Chakraborty and Ganguly (1992).

lation of the intracrystalline diffusion driven by garnet resorption. In the simulations, concentration changes inside a garnet undergoing resorption are computed and compared to measured zoning profiles, assuming that reaction takes place during cooling at a specified constant rate from a chosen initial temperature. The model seeks to achieve an optimal fit between the computed and measured zoning profiles by changing only a single input parameter, namely the temperature at which reaction begins.

**Summary of model.** The model approximates each natural garnet crystal as a sphere comprised of many concentric spherical shells of equal volume, each with uniform concentration. The initial temperature and a particular thermal history (cooling rate) are specified. Then the outermost shells are eliminated one-by-one, and the time required for each such volume decrement (which increases as temperature falls) is computed from relationships given below. For each increment of resorption, the flux of material into or out of the rim of the remaining crystal is determined by a retention/loss factor (see next paragraph) that ensures conformance with the material balance constraint provided by the measured total amount of each element in the relict crystal. The fluxes at all other boundaries between shells are governed by Fick's First Law. This resorption/diffusion cycle is repeated at successively later time steps and lower temperatures until the radius of the model crystal matches that of the relict crystal preserved in the natural texture.

Iterative calculation is required to determine the proper retention/loss factors. To begin, an initial trial value for each element is arbitrarily chosen. If, at the end of the simulation, the crystal is computed to contain an excess of that element over and above the total observed amount, then for the next iteration a smaller retention factor is chosen. Successive iterations converge upon the unique value that achieves material balance within a specified tolerance—in this case 0.05%.

**Model parameters.** Required inputs to the model are the form of the reaction rate law; the activation energy for intergranular diffusion of the element whose transport is rate-limit-

TABLE 1. — Extended

LU93-26c'		PH97-12a		PH97-12b		PH97-51a		PH97-51b		JS-6a		JS-6b	
Core	Rim	Core	Rim	Core	Rim	Core	Rim	Core	Rim	Core	Rim	Core	Rim
6.47	4.99	4.34	4.84	5.13	6.1	13.29	9.62	13.18	9.61	8.00	6.95	7.16	6.714
8.18	7.67	10.13	8.68	8.90	8.78	7.30	6.03	7.37	7.16	8.18	7.34	8.90	7.65
0.50	1.12	1.00	1.02	0.37	0.76	0.33	1.01	0.31	0.71	0.61	1.10	0.51	0.97
24.34	26.44	25.35	25.02	25.61	23.70	15.88	22.35	15.40	19.49	22.55	24.30	23.07	24.25
21.63	21.31	21.03	20.71	20.92	20.98	22.21	21.82	21.91	22.13	21.88	21.66	21.74	21.59
39.20	38.90	38.22	38.93	38.69	38.71	41.28	39.91	41.16	40.15	39.49	38.59	39.26	39.17
100.31	100.42	100.07	99.20	99.62	100.17	100.29	100.76	99.33	99.28	100.71	99.94	100.64	100.34
0.519	0.571	0.539	0.546	0.550	0.508	0.322	0.463	0.317	0.419	0.471	0.515	0.483	0.516
0.224	0.212	0.276	0.243	0.245	0.241	0.190	0.160	0.194	0.197	0.219	0.199	0.239	0.209
0.246	0.192	0.164	0.188	0.197	0.235	0.481	0.355	0.483	0.368	0.298	0.262	0.267	0.255
0.011	0.024	0.022	0.023	0.008	0.017	0.007	0.021	0.006	0.015	0.013	0.024	0.011	0.021

ing for the resorption reaction; temperature as a function of time during the resorption reaction; initial and final garnet radii; initial and final concentration profiles in the garnet; and rates of intracrystalline diffusion in garnet. All of these quantities are well-constrained, as described in the paragraphs that follow, but a sensitivity analysis is undertaken in a later section to assess the effects that uncertainties in input parameters have on the final results of the modeling.

**Form of reaction rate law.** As noted above, layered coronal textures are classic examples of reactions whose rates are limited by diffusion of elements through the intergranular medium across a growing product zone between reactants. Non-equilibrium thermodynamic models of the Llano coronas have identified Al as the element with the most restricted diffusion across the product zone (Carlson and Johnson 1991, p. 768), a finding that is quite general, as reported by Ashworth and Sheplev (1997, p. 3680). The kinetics of intergranular diffusion of Al are therefore regarded as rate-controlling for the resorption reaction. Diffusional control of the reaction kinetics justifies the assumption of an Arrhenius-style reaction rate law, in which the activation energy for intergranular diffusion of Al, symbolized here as  $Q_{IGD}$ , determines the temperature dependence of the rate of change of garnet volume  $[dV/dt]$ :

$$\left[ \frac{dV}{dt} \right] = \left[ \frac{dV}{dt} \right]_{t=0} \cdot \exp\left( \frac{-Q_{IGD}}{RT} \right). \quad (1a)$$

Because the integral of Equation 1a over the resorption interval must equal the total volume of garnet resorbed, the value of  $[dV/dt]_{t=0}$  is uniquely determined, for any chosen  $Q_{IGD}$  and thermal history, by the volume loss of the crystal  $\Delta V$ :

$$\left[ \frac{dV}{dt} \right]_{t=0} = \frac{\Delta V}{\int_0^{t_i} \exp\left( \frac{-Q_{IGD}}{RT(t)} \right) dt} \quad (1b)$$

in which the dependence of temperature on time is made explicit by denoting temperature as  $T(\tau)$ , and  $\tau_0$  is the time at which resorption is complete. In this work,  $\tau_0$  was chosen as the time at which  $T = 25^\circ\text{C}$ ; any time late in the process (when diffusion has become negligible) will yield the same result.

**Activation energy for intergranular diffusion of Al.** Experimental determination of the kinetics of intergranular diffusion under metamorphic conditions is extraordinarily difficult,

particularly in hydrous but fluid-undersaturated systems. Consequently, there are few relevant data, and none for Al. Fortunately, the only diffusional parameter required for this analysis is the activation energy, which varies, for dissolved cations in hydrothermal determinations, over little more a factor of two from one element to another (cf., Farver and Yund 2000b, and references therein). Considering the effects of charge and size of the diffusing species (Farver and Yund 1995a, p. 353), Si should be a suitable proxy for Al. Farver and Yund (2000b) measured an activation energy of 137 kJ/mol for grain-boundary diffusion of Si in a natural quartz aggregate under hydrothermal conditions, and an activation energy of 178 kJ/mol under completely anhydrous conditions. With these data as a guide, and considering the hydrous grain-boundary diffusion experiments of Farver and Yund to be the data most directly relevant to the circumstances governing corona formation in the Llano rocks, an activation energy for intergranular Al diffusion of 140 kJ/mol was chosen for the present modeling.

**Thermal history.** Temperature as a function of time during the resorption reaction is approximated by simple cooling at a fixed rate from an initial temperature, for which several justifications exist. Regionally, recrystallization during the corona-forming event is attributed to hydration at amphibolite grade associated with the intrusion of granitic plutons (Bebout and Carlson 1986); the subtlety of thermal aureoles surrounding these plutons (Letargo et al. 1995) indicates that the rocks were already hot when the intrusion/hydration episode began. Field and petrographic observations as described above are also consistent with a scenario in which hot but dry rock was prevented from reacting until small amounts of hydrous components gained access to reaction sites. The possibility of an appreciable increase of temperature or prolonged high temperature at the beginning of corona formation was considered but rejected on the basis of reconnaissance numerical simulations that demonstrated the impossibility of preserving sufficiently steep diffusion profiles for thermal histories of that kind in the temperature range indicated by exchange thermometry for coronal phases in nearby pelitic rocks.

The cooling rate used in the modeling was  $-10^\circ\text{C/m.y.}$ , based on the late-stage thermal histories for rocks in the northern Llano Uplift determined by Rougvie et al. (1999), who combined suites of radiometric ages with estimated closure

temperatures for various isotopic systems.

**Initial and final radii.** Initial radii for crystals were obtained from diameters measured petrographically and on BSE images, considering the original extent of the garnet to be the limit of the plagioclase + amphibole  $\pm$  magnetite layer in the corona (cf., Carlson and Johnson 1991). Several measurements ( $\sim 10$ – $12$ ) on each crystal were averaged to account for natural irregularities. Final radii were determined by the length of the microprobe traverses used to define the final concentration profiles.

**Final concentration profiles.** As detailed above, electron microprobe traverses were made from the centers of crystals to their rims: the crystal center was defined to be either the morphological center of the exposed central section through the crystal, or the maximum in Mn content for crystals with detectable residual growth zoning (which usually occurred very close to the morphological center).

**Initial concentration profiles.** Although the pre-resorption size of a partially reacted garnet can be recovered accurately from the coronal texture, original compositions in the portion of the garnet lost to resorption, and original compositions in the outer portion of the relict crystal, must be approximated by extrapolation from values in the inner, unaffected portion of the relict crystal. The specimens used in this analysis come from the western part of the Llano Uplift, a region that reached peak temperatures of  $\sim 750$  °C during the event in which garnet first crystallized, nearly sufficient to homogenize any original growth zoning in all but the largest crystals (Carlson and

Schwarze 1997). As a result, compositions in the interior portions of the relict crystals (portions unaffected by the resorption reaction) could be extrapolated with confidence to yield initial concentration profiles for use in the modeling (Fig. 11). For small crystals, initial profiles are very nearly flat, and for larger crystals, the profiles have gentle slopes compared with the slopes of the resorption-affected rims, so uncertainty produced by this extrapolation is minimal.

**Rates of intracrystalline diffusion.** The experiments of Chakraborty and Ganguly (1992), Ganguly et al. (1998), and other sources cited by these authors, provide data on tracer-diffusion coefficients in garnet for Mn, Fe, and Mg (and estimates for Ca). These data can be combined with the theoretical formulation of Lasaga (1979) for multicomponent diffusion in an ideal ionic solution to calculate diffusion rates for Mn, Fe, Mg, and Ca in garnet as a function of temperature, pressure, oxygen fugacity, and chemical composition.

For the purposes of this modeling, temperature was determined as a function of time by the chosen initial temperature and the specified cooling rate. Pressure was fixed at 3 kbar, in accordance with petrologic estimates for conditions during the recrystallization episodes responsible for garnet resorption (cf. Carlson 1998, p. 19). Oxygen fugacity during the resorption event was constrained by the ubiquitous presence of magnetite in the coronal reaction textures. A value corresponding to the center of the magnetite stability field was assumed, and the ratio of model oxygen fugacity to the oxygen fugacity defined by the graphite-CO<sub>2</sub> equilibrium was therefore fixed at 0.1936.

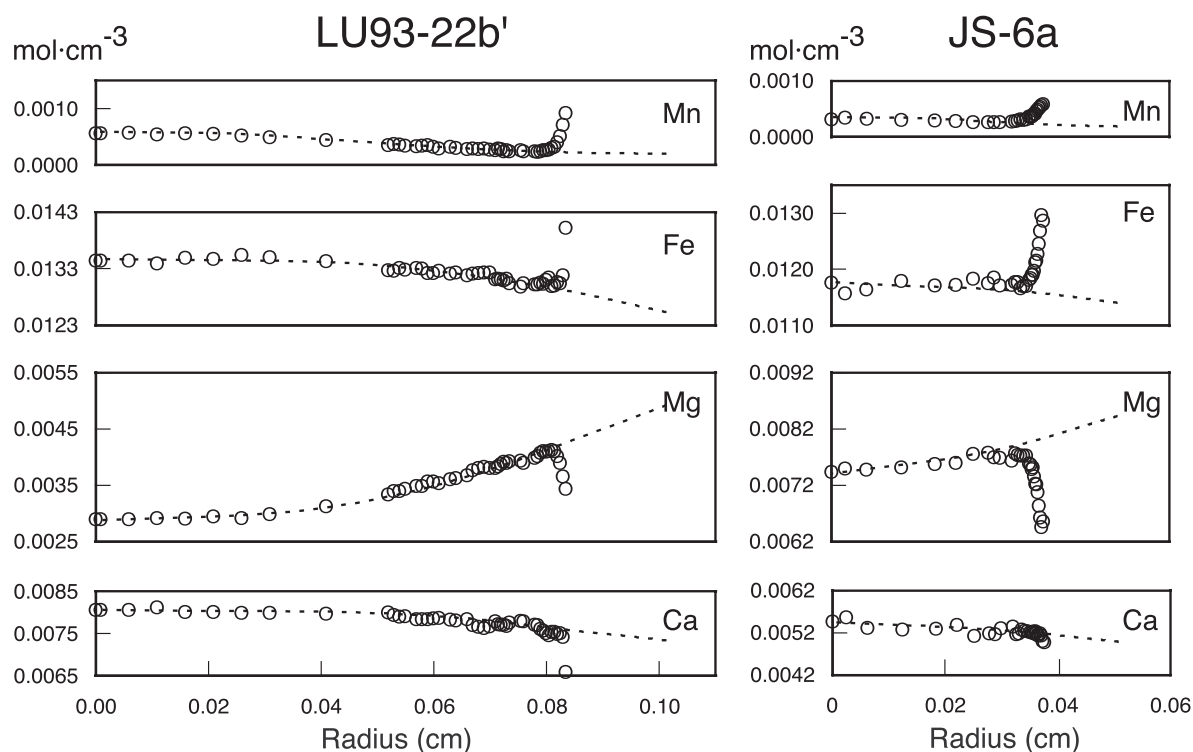


**FIGURE 11.** Examples of extrapolations of unaffected portions of compositional profiles in relict crystals. Circles are microprobe analyses; dotted lines are extrapolations made to approximate the pre-resorption zoning profiles. Radial limit of extrapolation is determined from petrographic measurement of original crystal size.

The experimental approach of Chakraborty and Ganguly (1992) and Ganguly et al. (1998), and the multicomponent diffusion theory of Lasaga (1979), include the dependence of diffusion on composition within the range of variation encountered in the diffusion experiments: although each tracer diffusion coefficient  $D_i^*$  is regarded as independent of composition within any experimental diffusion couple, the multicomponent diffusion matrix incorporates an explicit dependence on composition. Importantly, however, the large differences between experimental determinations for tracer diffusion coefficients in spessartine-almandine and pyrope-almandine diffusion couples warn one to expect uncertainty in extrapolation of rates to natural specimens whose compositions depart significantly from those used in the experiments. The garnets studied in this effort are principally in the range  $\text{Alm}_{32-59}\text{Sps}_{1-4}\text{Grs}_{16-32}\text{Pyp}_{12-48}$  (Fig. 10), and thus contain substantially more Ca than any experimentally studied composition, and more Mg than the almandine-spessartine couples used by Chakraborty and Ganguly (1992).

In this modeling, values for the tracer diffusion coefficients were selected as follows. For a set of preliminary models, the data for spessartine-almandine couples in Chakraborty and Ganguly (1992) were used; these data were preferred over those of Ganguly et al. (1998) because of the closer correspondence of molar volumes for these compositions to the molar volumes for the Llano garnets. It was immediately apparent from this preliminary modeling that the natural profiles provide very tight constraints on *relative* rates of intracrystalline diffusion. However, it was also clear that, using the tracer coefficients from the literature, it would be impossible to fit simultaneously all four of the resorption profiles in any one crystal: thermal histories that generated good fits for Mn, for example, produced insufficient diffusional transport of Fe, Ca, and especially Mg (Fig. 12).

Based on the preliminary models, a set of tracer diffusion coefficients (Table 2, Fig. 13) was chosen to enforce compliance with the observed *relative* rates of diffusion in the natural occurrences. This choice required virtually no change in values of the tracer diffusion coefficient for Mn, a small adjustment to the literature values for Fe, and a larger modification of the published values for Mg. The preferred tracer diffusion coefficients determined in this way for Mn and Fe fall within the range of uncertainty of extrapolation of the published experimental values (95% confidence interval). The preferred values for Mg diffusion, however, fall slightly outside the bounds of extrapolated experimental uncertainty. A likely reason for this is the high value for the activation energy for Mg tracer diffusion (67 997 kcal/mol) given in Chakraborty and Ganguly (1992) for spessartine-almandine couples. This is larger than the activation energies determined in that study for Mn and Fe (60 569 and 65 824 kcal/mol, respectively), and seems anomalously high in comparison with the activation energy for Mg tracer diffusion (60 760 kcal/mol) determined for pyrope-almandine couples by Ganguly et al. (1998). The relative rates of intracrystalline diffusion for Mn and Mg derived from the present modeling are consistent with the notion that the activation energy for  $D_{\text{Mg}}^*$  in the spessartine-almandine experiments is erroneously high; in fact, if the activation energy

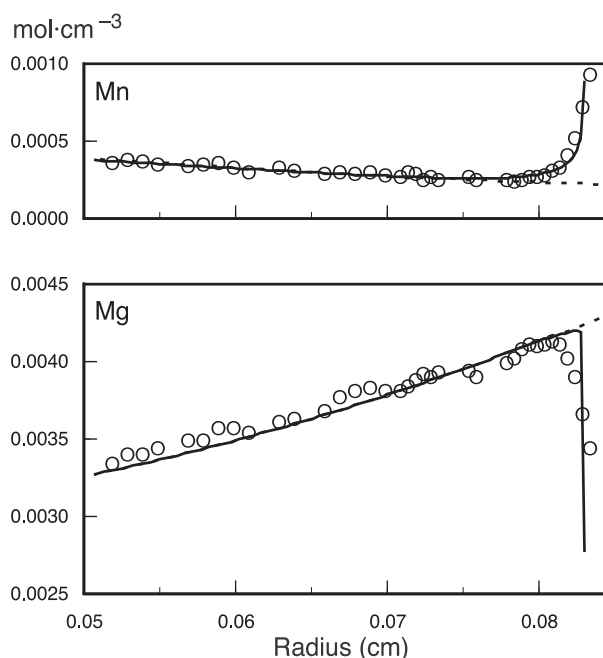


**FIGURE 12.** Unsuccessful attempt to fit stranded intracrystalline diffusion profiles using tracer diffusion coefficients directly from Chakraborty and Ganguly (1992). Circles are microprobe analyses; dotted lines are extrapolations; and solid lines are the results of the numerical models. A model with an initial temperature that gives a reasonably good fit to the Mn profile (top) calculates insufficient outward transport of Mg (bottom). Too little Mg is supplied from the interior, so too much must be removed from the outermost periphery; the result is a profile that is too steep and with a rim concentration much lower than the one actually measured.

**TABLE 2.** Intracrystalline tracer diffusion coefficients

	$D_0$ ( $\text{cm}^2/\text{s}$ )	$Q$ (cal/mol)	$\Delta V^*$ ( $\text{cm}^3/\text{mol}$ )
$D_{\text{Mn}}^*$	0.003518	64,000	6.04
$D_{\text{Fe}}^*$	0.001776	64,000	5.63
$D_{\text{Mg}}^*$	0.004067	64,000	5.27
$D_{\text{Ca}}^*$	0.004079	64,000	6.04

Note: Values of  $D^*(P, T)$  used in this study were computed by inserting the values above into Equation 3 of Chakraborty and Ganguly (1992), then correcting the result for oxygen fugacity. Symbols match those of Chakraborty and Ganguly (1992).

for  $D_{\text{Mg}}^*$  in the pyrope-almandine experiments is instead used to extrapolate down-temperature, the preferred value used in this study falls comfortably within the bounds of experimental uncertainty.

#### Extraction of intergranular diffusivity for Al

The effective intergranular diffusivity of Al (symbolized here as  $D_{\text{Al}}^{\text{eff}}$ ) can be estimated by equating the measured length scale for intergranular diffusion in the coronal textures with the characteristic diffusion distance  $x$ , which for an isothermal diffusion episode is defined here by  $x \equiv (D_{\text{Al}}^{\text{eff}} t)^{1/2}$ . This characteristic diffusion distance, or “penetration depth,” is a measure of the mean distance traveled by diffusing atoms (cf., Christian 1975, p. 386), and is used here in keeping with the formulation of Ashworth (1993, p. 336).

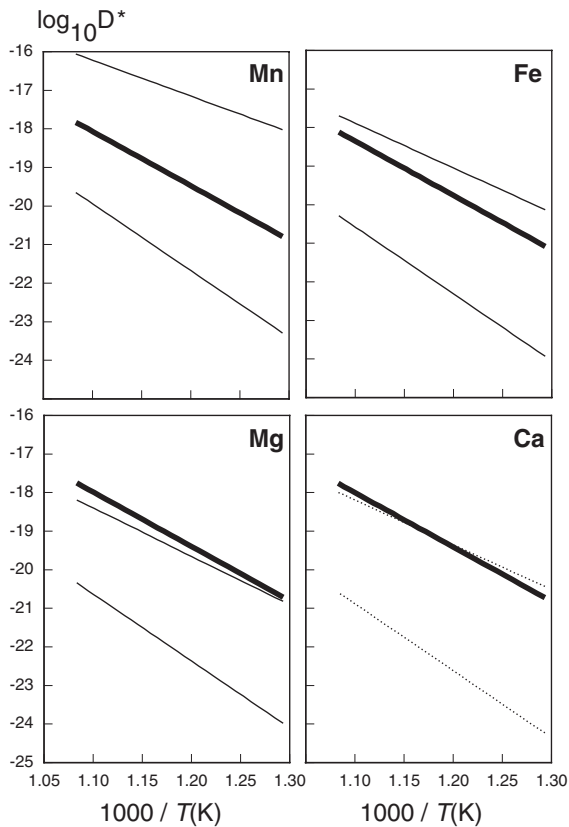


**FIGURE 13.** Tracer diffusion coefficients from 650 to 500 °C, at 3 kbar and an oxygen fugacity at the center of the magnetite stability field. Bold lines are the preferred values used in this study to produce relative rates of intra-crystalline diffusion consistent with measured profiles. Light lines (Mn, Fe, Mg) represent the limits of 95% confidence intervals around a line regressed through the data of Chakraborty and Ganguly (1992), after correction to the same pressure and oxygen fugacity. Thus their expression for  $D^*$  would give lines that pass through the center of each field bounded by light lines, but the range of experimental uncertainty includes the entire field. Ca lines are dotted, to emphasize that the experimental data place few constraints on these values; the dotted lines here are based on  $D_{Ca}^* = 0.5 D_{Fe}^*$  (Chakraborty and Ganguly 1992, p. 81).

To account for the change in temperature during corona formation, this relationship is re-cast as

$$x^2 = \int_0^{t_f} \left[ D_{\infty, Al}^{\text{eff}} \cdot \exp\left(\frac{-Q_{IGD}}{R T[t]}\right) \right] dt \quad (2)$$

in which the value of  $x$  is taken as the distance between the surfaces of the reactants in the corona when reaction ceased (that is, the distance now measured from BSE images), and  $D_{Al}^{\text{eff}}$  has the standard Arrhenius-style dependence on temperature through the activation energy for its intergranular diffusion  $Q_{IGD}$ . Equation 2 is solved numerically for  $D_{\infty, Al}^{\text{eff}}$ .

(The quantity symbolized here by  $D_{Al}^{\text{eff}}$  is referred to as the “effective diffusivity,” because it can be argued that this quantity is not strictly an effective diffusion coefficient, owing to its dependence on the solubility of Al in the intergranular medium. One might instead choose to designate this quantity as

an “effective transport coefficient,” but that term could carry an unintended connotation of the combined effect of diffusive and advective transport mechanisms. The term “effective diffusivity” is chosen for its simplicity, and its meaning here is unambiguously defined by Eq. 2.)

## Results

Fourteen compositional profiles were modeled, selected from specimens that represent a wide range of possible resorption histories, in order to assess the uncertainties that arise from natural variations. The effects of crystal size and degree of resorption were explored, and the extent of variation was examined within individual crystals, between crystals in the same thin section, among various outcrops in a single locality, and between a pair of different localities. Despite this attempt to uncover possible sources of variability, all fourteen modeled profiles yielded very similar results, indicating that the approach is both robust and precise.

The list of analyzed profiles in Table 3 spans a wide range of crystal size (0.05–0.33 cm initial diameter) and includes degrees of resorption ranging from moderate to extensive (36–82% volume loss). Profiles with identifiers that differ only in the presence or absence of a final “prime” (e.g., LU93-22a and LU93-22a') were measured in separate locations on the same crystal. The two JS profiles were measured on different crystals in the same thin section, as were the two PH97-12 profiles and the two PH97-51 profiles. Specimens LU93-22a and LU93-22b come from the same outcrop, as do specimens LU93-26b and LU93-26c. The two specimens with prefix JS were collected from a metamafic occurrence separated by 2 km from the group of outcrops that yielded the PH and LU specimens, all of which came from within about 0.5 km of one another.

Two representative comparisons of measured and modeled compositional profiles appear in Figure 14—one for a large crystal with relatively little resorption, the other for a crystal of moderate size with relatively greater resorption. The remaining 12 fits are similar in quality to the two shown. Fitting was done by adjustment of only one of the model parameters, namely the temperature at the onset of resorption; all other parameters are identical in all 14 fits. Table 3 includes the best-fit value for this initial temperature for all modeled profiles.

Also listed in Table 3 is a general indication of the duration of the resorption reaction as computed by the model. The duration given there serves only to provide an approximate sense of the overall time scale, insofar as the Arrhenius relations used for diffusion allow for continued reaction and intracrystalline diffusion (at exponentially declining rates) at all temperatures, so that the final state is approached only asymptotically. Figure 15 illustrates the decline in the rate of resorption over time for a representative example. In Table 3, the duration of the reaction is indicated by the time required to accomplish 95% of the measured garnet volume loss. Note that this time is *not* used to retrieve values for  $D_{\infty, Al}^{\text{eff}}$ ; numerical solution of the integral in Equation 2 allows for analysis of the entire resorption interval, including the asymptotically declining effects at low temperature, to any desired degree of precision.

The final entries in Table 3 are the values for the pre-expo-

**TABLE 3.** Results of best-fit simulations and computed intergranular diffusivity for Al

Traverse	$r_i$ (cm)	$r_f$ (cm)	$\Delta V$ (%)	$T_i$ (°C)	$t_{95}$ (m.y.)	$x$ (cm)	$\log_{10} D_{\text{res}}^{\text{eff,Al}}$ ( $D$ in $\text{m}^2/\text{s}$ )	$\log_{10} D_{575,\text{Al}}^{\text{eff}}$ ( $D$ in $\text{m}^2/\text{s}$ )
LU93-22a	0.1481	0.1195	-47.5	630	11.5	0.0536	-12.6	-21.2
LU93-22a'	0.1405	0.1119	-49.5	640	11.8	0.0536	-12.7	-21.3
LU93-22b	0.1015	0.0836	-44.0	640	11.8	0.0329	-13.1	-21.7
LU93-22b'	0.1013	0.0834	-44.3	620	11.3	0.0329	-12.9	-21.5
LU93-26b	0.0734	0.0591	-47.8	625	11.4	0.0315	-13.0	-21.6
LU93-26b'	0.0758	0.0616	-46.5	630	11.5	0.0315	-13.0	-21.7
LU93-26c	0.0854	0.0628	-60.2	645	11.9	0.0308	-13.2	-21.8
LU93-26c'	0.0853	0.0627	-60.3	640	11.8	0.0308	-13.2	-21.8
PH97-12a	0.1629	0.1400	-36.5	625	11.4	0.0505	-12.6	-21.2
PH97-12b	0.1490	0.1200	-47.8	635	11.6	0.0501	-12.7	-21.3
PH97-51a	0.0289	0.0196	-68.8	620	11.3	0.0149	-13.6	-22.2
PH97-51b	0.0253	0.0143	-81.9	610	11.1	0.0165	-13.4	-22.0
JS-6a	0.0508	0.0376	-59.5	625	11.4	0.0188	-13.4	-22.1
JS-6b	0.0660	0.0509	-54.0	610	11.1	0.0214	-13.2	-21.8
Mean							-13.0	-21.7
e.s.d.							0.3	0.3

Notes:  $r_i$ ,  $r_f$  = initial, final garnet radii;  $\Delta V$  = volume change for garnet;  $T_i$  = temperature at onset of resorption used in best-fit simulation;  $t_{95}$  = time required in simulation to achieve 95% of total resorption;  $x$  = width of coronal reaction zone;  $D_{\text{res}}^{\text{eff,Al}}$  = pre-exponential quantity in Arrhenius expression for rate of effective intergranular diffusion of Al;  $D_{575,\text{Al}}^{\text{eff}}$  = intergranular diffusivity of Al at 575 °C.

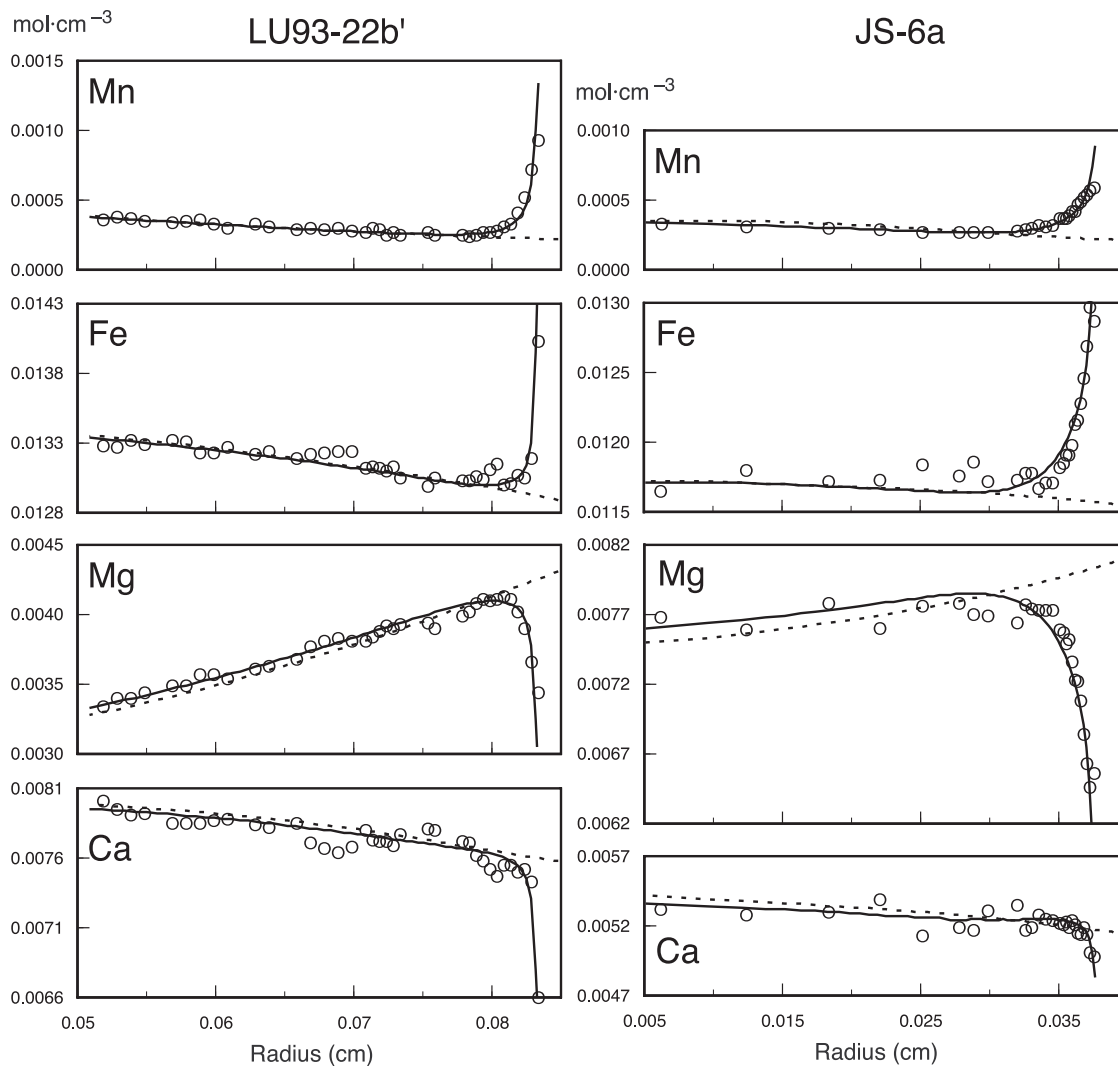


**FIGURE 14.** Representative fits of modeled diffusion profiles to measured compositions in relict garnet. Circles are microprobe analyses; dotted lines are extrapolations used to estimate original profiles; and solid lines are the results of the numerical simulations. Horizontal and vertical axes are scaled identically for all diagrams, so distances and slopes are directly comparable.

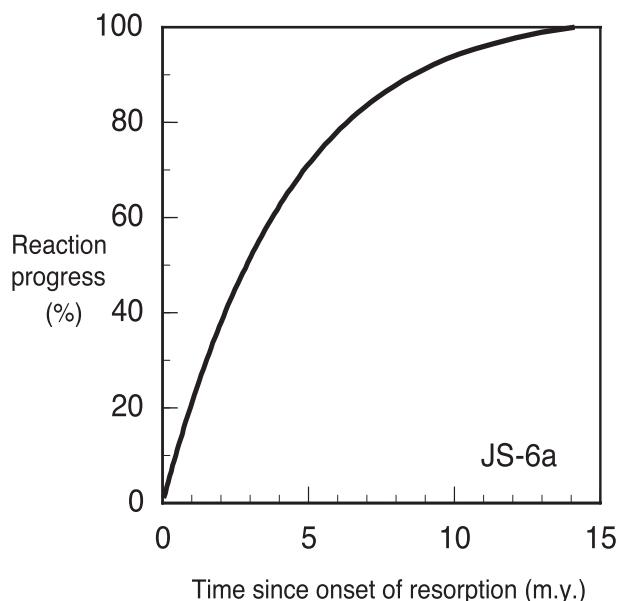


**FIGURE 15.** Cumulative percent of total garnet resorption (on volume basis) as a function of time in representative model. During the time interval shown, temperature declines from 625 to ~475 °C, producing an exponential decrease in reaction rate. As a result, although half of the total reaction occurs in the first 3 m.y., more than 11 m.y. are required to reach 95% completion.

nential constant  $D_{\text{Al}}^{\text{eff}}$  for intergranular diffusivity of Al, and the value of the diffusivity calculated at 575 °C. This reference temperature is near the center of the range over which resorption and diffusion took place in the Llano rocks, and falls between the formation temperatures of  $550 \pm 100$  and  $600 \pm 100$  °C assigned to the two coronas studied by Ashworth (1993, p. 333), which facilitates comparison with those prior results.

**Precision and Accuracy.** The calculations involved in the fitting procedure are too complex to permit determination of uncertainties by statistically rigorous propagation of errors. In lieu of such an approach, the level of uncertainty in the derived values can be assessed on the basis of the degree of scatter in the computed results and on the basis of a sensitivity analysis that evaluates the effect on the results of perturbing each of the input parameters.

**Scatter.** The computed values for the base-10 logarithm of the intergranular diffusivity at 575 °C in Table 3 cluster tightly, with a mean value of  $-21.7$  e.s.d. 0.3. The variation for two traverses on a single crystal is as large as any other variation in the data set, despite the fact that the set of traverses involves different crystals, different specimens, different outcrops, and different localities. The inherent precision of the technique thus appears to be on the order of  $\pm 0.3$  log units for  $D_{\text{Al}}^{\text{eff}}$ , or roughly plus-or-minus a factor of two.

**Sensitivity analysis.** A measure of the accuracy of the results can be obtained by evaluating the sensitivity of the final result to perturbations of the input parameters. In this process, the data for specimen LU96-26c' were repeatedly re-fit, modi-

fying the input parameters in the best-fit model one-by-one. Each parameter was increased, then decreased, by an amount representing its estimated uncertainty, while holding all other input parameters unchanged. Pressure was altered by  $\pm 0.5$  kbar; initial temperature by  $\pm 10$  °C; the activation energy for intergranular diffusion by  $\pm 50$  kJ/mol; the cooling rate by a factor of two; and oxygen fugacity by a factor of ten.

As shown in Table 4, none of these sources of uncertainty produces effects that exceed the small natural variability established above by comparison of different traverses, different crystals, different specimens, different outcrops, and different localities. Thus the uncertainties in input parameters, other than the intracrystalline diffusion coefficients, do not add appreciably to the uncertainty expressed by the dispersion among the results in Table 3.

The final result is, however, quite sensitive to the values chosen for rates of intracrystalline diffusion, so the required extrapolation of experimental rates could potentially introduce very large uncertainties into the computation of intergranular diffusivities. Fortunately, this is not the case, because petrologic considerations provide a helpful constraint on intracrystalline diffusion rates, as described immediately below.

**Accuracy from petrologic constraint.** Because this approach is essentially an assessment of the relative rates of intergranular and intracrystalline diffusion, one might expect that estimates of intergranular diffusivities could be no more accurate than the expected errors in the extrapolated experimental measurements of intracrystalline diffusion. Thus, because the confidence intervals in Figure 13 span 2–5 orders of magnitude, one might expect that the uncertainty in the calculated intergranular diffusion coefficients must be just as large. And this would be true, were it not for the existence of an important further constraint: although the temperature at the onset of resorption ( $T_i$ ) was allowed in the modeling to assume any value required to produce a good fit to the measured compositional profiles, in fact that temperature is constrained petrologically. Garnet-biotite thermometry for reaction zones around garnet in pelitic rocks in the LU/PH locality, combining garnet rim compositions with compositions of neighboring biotite, yields  $612 \pm 25$  °C via the calibration of Holdaway (2000).

But much of the range encompassed by the confidence intervals in Figure 13 is inconsistent with this constraint. On the one hand, intracrystalline diffusion rates near the bottom of the confidence intervals would require temperatures for corona formation far in excess of the thermometric estimate (probably inconsistent with the thermal stability of amphibole in the coronas); on the other hand, intracrystalline diffusion rates near the top of confidence intervals would require that corona formation was initiated at temperatures significantly lower than that recorded by the garnet-biotite exchange reaction.

The constraint imposed by petrologic evidence is shown in Figure 16 by indicating the value of  $T_i$  that would be necessary to fit the data for specimen JS-6a using different values for intracrystalline diffusion rates. This specimen yielded a temperature for the onset of reaction ( $T_i$ ) of 625 °C, at the center of the total range of 610–640 °C (Table 3). Error assessment based on Figure 16 is complicated, of course, by the likelihood that corona formation was first initiated at a temperature higher by

some unknown amount than that recorded by closure of the garnet-biotite Fe-Mg exchange system, and by the impossibility of knowing exactly where along the path of the asymptotic decline of coronal-reaction progress the garnet-biotite exchange reaction ultimately closed. Nevertheless, values for the intracrystalline diffusion coefficients that differ from the preferred values by more than 0.5 or perhaps 1.0 log unit are likely to be inconsistent with the petrologic evidence. For example,

**TABLE 4.** Sensitivity analysis

Perturbation	$T_i$ (°C)	$\Delta \log_{10} D_{T,Al}^{eff}$ ( $D$ in $m^2/s$ )
$T$ +10 °C	655	-0.09
$T$ -10 °C	635	+0.10
$P$ +0.5 kbar	645	+0.00
$P$ -0.5 kbar	645	-0.00
$f_{O_2}$ $\times 10$	635	+0.09
$f_{O_2}$ $\times 0.1$	655	-0.10
$dT/dt$ $\times 2$	660	-0.14
$dT/dt$ $\times 0.5$	630	+0.15
$Q_{GD}$ +50 kJ/mol	640	+0.05
$Q_{GD}$ -50 kJ/mol	650	-0.05

if the preferred values for intracrystalline diffusion used in this study were too low by 0.5 (or 1.0) log unit, then one would have to accept that in rocks undergoing reaction beginning at 597 °C (or 571 °C) and cooling at 10 °C/m.y., coronal garnet-biotite pairs record closure at  $612 \pm \sim 25$  °C. Conversely, if the preferred values for intracrystalline diffusion used in this study were too high by 0.5 (or 1.0) log unit, then one would have to accept that in rocks undergoing reaction beginning at 655 °C (or 686 °C) and cooling at 10 °C/m.y., garnet-biotite pairs record closure at  $612 \pm \sim 25$  °C. Whereas the above scenarios based on an error of  $\pm 0.5$  log unit are not difficult to rationalize, those based on an error of  $\pm 1.0$  log unit border on the improbable, and scenarios based on larger errors seem implausible. The estimated intergranular diffusivity for Al given in the following equation, applicable to hydrous but fluid-undersaturated systems, is therefore probably accurate to within  $\pm 0.5$  log unit, or perhaps  $\pm 1.0$  log unit, in the range of temperature encompassed in these models, roughly 650–500 °C:

$$D_{T,Al}^{eff} (m^2/s) = 1.0 \times 10^{-13} \cdot \exp\left(\frac{-140 \text{ kJ/mol}}{RT}\right). \quad (3)$$

### Discussion

The coupling between intracrystalline and intergranular diffusion in these coronal textures, together with the constraints provided by their petrologic and geologic setting, lead to improvements in the accuracy and precision of estimates for the rates of both processes in nature, as described below. The well-constrained estimate in this study for rates of intergranular diffusivity of Al in fluid-undersaturated systems lends credibility to earlier, less-certain estimates in fluid-saturated systems. In combination, the two sets of estimates appear to bracket rates in natural occurrences, opening the door to quantitative evaluation of time and length scales of equilibration by diffusive processes in metamorphic rocks.

**Implications for rates of intracrystalline diffusion.** The large extrapolations in temperature required to apply the experimental data of Chakraborty and Ganguly (1992) to common metamorphic environments generate wide ranges of uncertainty. But the present work demonstrates that only a limited set of possible values for the tracer diffusion coefficients is consistent with petrologic constraints on the temperature of corona formation and with the observed *relative* rates of intracrystalline diffusion for different elements. The preferred values of the intracrystalline tracer diffusion coefficients given in Table 2 and shown in Figure 13 for Fe and Mg, although largely consistent with the high-temperature experiments, are more likely to be applicable to metamorphic systems than direct extrapolation of the experimental data, which would give values in the center of each confidence interval; preferred values for Mn differ little from the experimental extrapolation. An unexpected bonus derived from the numerical simulations was the set of very tight constraints on the *relative* rates of intracrystalline diffusion of different elements in garnet. This result permitted extraction of new values for the intracrystalline diffusivity of Ca, which is largely unconstrained by published experiments. Notably, rates of diffusion for different elements using the diffusion parameters in Table 2 are closer to one another than are the experimental extrapolations, which might be

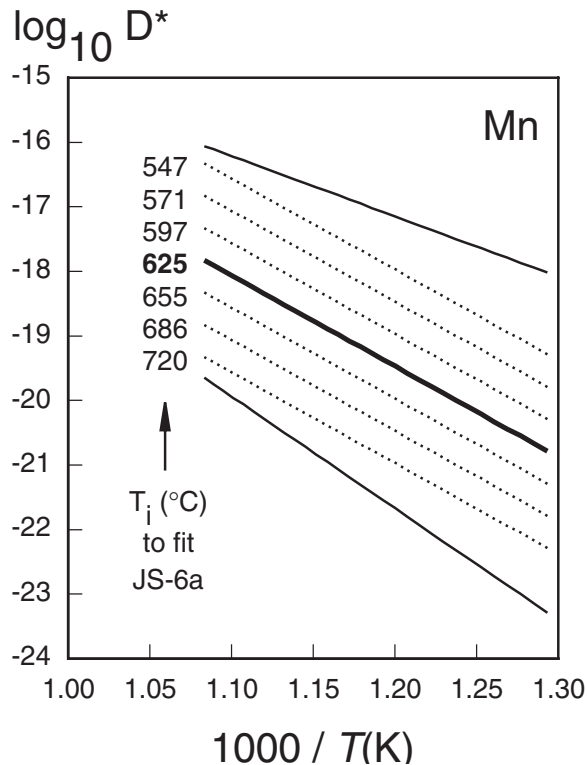


**FIGURE 16.** Petrologic constraint on rates of intracrystalline diffusion (650 to 500 °C, 3 kbar, center of magnetite stability field). As in Figure 13, bold line shows preferred values for diffusivity used in this study and light lines are 95% confidence intervals around the regression line of Chakraborty and Ganguly (1992). Dotted lines are contours of higher and lower diffusivities at 0.5 log-units spacing. The number shown at the end of each dotted line is the value for the temperature at the onset of resorption ( $T_i$ ) that would be required to fit the compositional profile of specimen JS-6a using those diffusion data. As discussed in text, petrologic constraints on the temperature of corona formation make it unlikely that actual diffusivities differ from those shown by the bold line by more than 0.5 or perhaps 1.0 log unit.

in part the result of down-temperature propagation of small errors in the experimentally determined activation energies; it might also be in part the result of the natural compositions lying closer to the center of the garnet quaternary.

An important consideration is that the intracrystalline diffusion coefficients derived here were obtained in compositions with appreciable fractions of the grossular component. Given the clear dependence of diffusivity on composition evident in experiments, care should be taken in extrapolating these data to other compositions. In particular, Ca diffusion may be much slower in compositions closer to the almandine-pyropite join: reconnaissance modeling of garnet resorption in pelitic rocks from the Llano Uplift indicates that the ratio between rates of Ca and Fe diffusion is indeed significantly lower than in more-calcic garnet in mafic rocks.

**Implications for rates of intergranular diffusion.** Very few quantitative estimates exist of the effective intergranular diffusivity of Al in nature, so there are few standards against which the results of this study, represented by Equation 3 above, can be judged. Most directly comparable is the determination of Ashworth (1993), who used features of two layered coronal textures to evaluate  $D_{Al}^{eff}$  at 550–600 °C; he obtained a value of  $10^{-24\pm 2}$  m<sup>2</sup>/s. The large uncertainty attached to this result derives from the difficulty of constraining the duration of the corona-forming event, and is quite conservative: Ashworth (1993, p. 334) stated, “To avoid any spurious impression of accuracy, a generous range of uncertainty (1–100 m.y.) is adopted for the time scale available for reaction...”. For comparison, at 575 °C, Equation 3 gives  $D_{Al}^{eff} = 10^{-21.7\pm 0.5}$  m<sup>2</sup>/s (any potentially spurious impression of accuracy here should be mitigated by the comments at the end of the foregoing results section!); this value barely overlaps the upper limit of the range derived in the study of Ashworth. Intriguingly, this result may have been presaged by Ashworth and Sheplev (1997), whose efforts to quantify coronal reaction affinities led them to the conclusion (p. 3682) that “only the highest parts of the Ashworth (1993) ranges of estimated  $D_{Al}$  are acceptable.” This study and those of Ashworth (1993) and Ashworth and Sheplev (1997) therefore appear to have converged on a consistent result.

These findings may be contrasted with available information, again limited, on intergranular diffusivities for Al in fluid-saturated systems. Carlson et al. (1995) presented numerical simulations of prograde crystallization events in which models of diffusion-controlled nucleation and growth of porphyroblasts were fitted to observed crystal size distributions and measures of spatial ordering and clustering. Adjusting those results to take advantage of recent data on activation energies requires recalculation using a value of 140 kJ/mol (the original value was 84 kJ/mol). An average of the four determinations made in that work yields the following equation for the intergranular diffusivity of Al in these presumably fluid-saturated systems:

$$D_{T,Al}^{eff} (\text{m}^2/\text{s}) = 3.0 \times 10^{-11} \cdot \exp\left(\frac{-140 \text{ kJ/mol}}{R T}\right). \quad (4)$$

On this basis, the best-fit values for  $D_{Al}^{eff}$  in m<sup>2</sup>/s at 575 °C range from  $10^{-19.6}$  to  $10^{-18.8}$  and average  $10^{-19.1}$ . Thus diffusivities of Al at this temperature are computed to differ by about 2.6

log units between fluid-saturated and fluid-undersaturated environments, with diffusion more rapid in the presence of a fluid phase along grain edges. A difference of this magnitude is consonant with, though somewhat larger than, the divergence between hydrothermal and dry experiments on Si diffusion in quartz aggregates performed by Farver and Yund (2000b), whose diffusivity data predict a difference of 1.3 log units at 575 °C in that system.

Overall, the relative rates determined by the completely different methods employed in this study and that of Carlson et al. (1995)—but by analysis of natural textures in both instances—appear to be consistent with one another and with available data from other sources. They should, therefore, constitute a reasonably well-constrained bracket for rates of Al diffusion in nature, in fluid-saturated and fluid-undersaturated systems.

**Implications for metamorphic equilibration.** Figure 17 explores the implications of these findings for scales of dis-

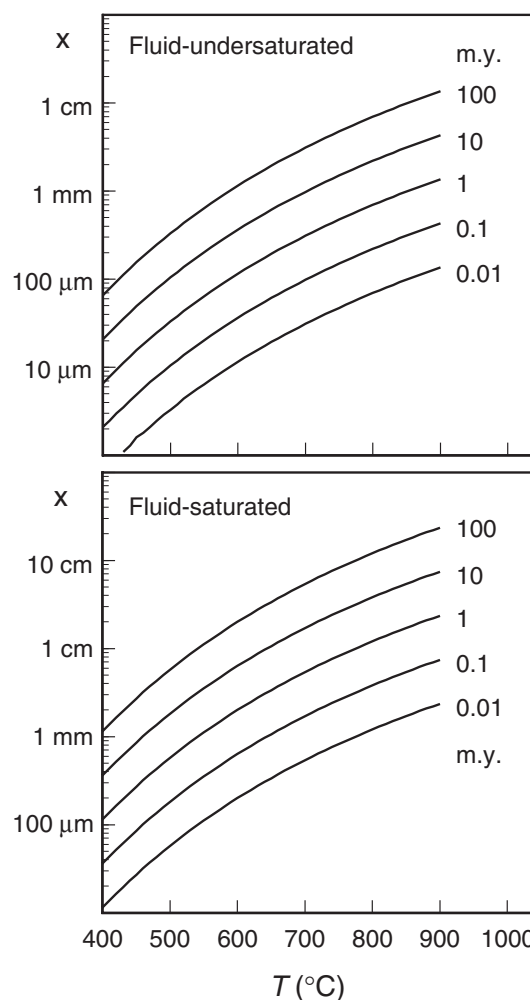


**FIGURE 17.** Characteristic diffusion distances for Al in fluid-undersaturated and fluid-saturated systems as a function of time and temperature, calculated from Equations 3 and 4 of the text.

equilibrium and rates of equilibration during metamorphism. The data obtained from natural occurrences in the range 500–650 °C have been extrapolated across a wider temperature range via Equations 3 and 4, and characteristic diffusion distances for Al have been computed according to  $x = (D_{Al}^{eff} \cdot t)^{1/2}$ . For processes governed by Al diffusion—a spectrum that includes the crystallization of many common porphyroblasts at one end, and the development of coronal reaction textures at the other, with much in between—Figure 17 can be used to estimate the length scale over which Al diffusion should be effective for a given thermal history, or conversely can be used to estimate the time scales needed to redistribute Al across a chosen distance in a given thermal regime.

Carmichael (1969) described the importance to metamorphic reaction mechanisms of the relatively slow intergranular diffusion of Al compared to other major elements. In a similar vein, the present work makes it clear that the relative rates of intergranular diffusion of a variety of major and trace elements exert fundamental control on the ability of metamorphic rocks to achieve chemical equilibrium. If the notions developed in Part I of this address are given credence, then over much of the range of temperatures that characterizes metamorphism in the crust, Al occupies a pivotal position in the realm of intergranular diffusion kinetics. Most abundant univalent and divalent cations—except perhaps for Mn in the lowest greenschist facies and Ca below the upper amphibolite facies—diffuse through the intergranular medium significantly more rapidly than does Al, and are capable of equilibration over much larger length scales. Most trivalent, quadrivalent, and pentavalent cations, on the other hand, diffuse significantly more slowly, some more slowly than Al, and should be expected to equilibrate across much shorter distances. The present data therefore provide limits on diffusivities for these other categories of elements as well. With due attention to the complexities introduced by variable fluid chemistry, oxidation state, and alternative transport mechanisms such as advective fluid flow, the relationships depicted in Figure 17 should provide a useful quantitative framework for determining scales of disequilibrium and rates of equilibration during metamorphism.

#### ACKNOWLEDGMENTS

This work was supported by NSF grant EAR-9902682, and benefited from NSF support of the University of Texas High-Resolution X-ray CT Facility (EAR-981020, EAR-0004082). Additional assistance from the Geology Foundation of the University of Texas at Austin is gratefully acknowledged. I thank David Hirsch and Richard Ketcham for assistance with and contributions to the computer programming effort; Richard Ketcham for assistance in collection of the X-ray CT data; and Cambria Denison and Jaime Barnes for collection of some of the electron-microprobe data. I am especially grateful to Toby Rivers, Jibamitra Ganguly, David Hirsch, and Richard Ketcham, who provided timely and thought-provoking comments on the manuscript.

#### REFERENCES CITED

- Anderson, S.D. (2001) High-pressure metamorphism in the western Llano Uplift recorded by garnet-clinopyroxenes in Mason County, Texas. MS Thesis, University of Texas at Austin, 221 p.
- Ashworth, J.R. (1993) Fluid-absent diffusion kinetics of Al inferred from retrograde metamorphic coronas. *American Mineralogist*, 78, 331–337.
- Ashworth, J.R. and Birdi, J.J. (1990) Diffusion modelling of coronas around olivine in an open system. *Geochimica et Cosmochimica Acta*, 54, 2389–2401.
- Ashworth, J.R. and Chambers, A.D. (2000) Symplectic reaction in olivine and the controls of intergrowth spacing in symplectites. *Journal of Petrology*, 41, 285–304.
- Ashworth, J.R. and Sheplev, V.S. (1997) Diffusion modelling of metamorphic layered coronas with stability criterion and consideration of affinity. *Geochimica et Cosmochimica Acta*, 61, 3671–3689.
- Barnes, J.D. and Carlson, W.D. (2001) Major- and trace-element zoning as a function of garnet crystallization temperature. Geological Society of America, South-Central Section, Abstracts with Programs, 33, 56–57.
- Bebout, G.E. and Carlson, W.D. (1986) Fluid evolution and transport during metamorphism: Evidence from the Llano Uplift, Texas. *Contributions to Mineralogy and Petrology*, 92, 518–529.
- Brady, J.B. (1983) Intergranular diffusion in metamorphic rocks. *American Journal of Science*, 283A, 181–200.
- Carlson, W.D. (1989) The significance of intergranular diffusion to the mechanisms and kinetics of porphyroblast crystallization. *Contributions to Mineralogy and Petrology*, 103, 1–24.
- (1998) Petrologic constraints on the tectonic evolution of the Llano Uplift. In M.C. Gilbert, and J.P. Hogan, Eds. *Basement Tectonics* 12, p. 3–27. Kluwer Academic Press, Dordrecht.
- Carlson, W.D. and Denison, C. (1992) Mechanisms of porphyroblast crystallization: Results from high-resolution computed X-ray tomography. *Science*, 257, 1236–1239.
- Carlson, W.D. and Johnson, C.D. (1991) Coronal reaction textures in garnet amphibolites of the Llano Uplift. *American Mineralogist*, 76, 756–772.
- Carlson, W.D. and Schwarze, E.T. (1997) Petrologic significance of prograde homogenization of growth zoning in garnet: An example from the Llano Uplift. *Journal of Metamorphic Geology*, 15, 631–644.
- Carlson, W.D., Denison, C., and Ketcham, R.A. (1995) Controls on the nucleation and growth of porphyroblasts: Kinetics from natural textures and numerical models. *Geological Journal*, 30, 207–225.
- Carmichael, D.M. (1969) On the mechanism of prograde metamorphic reactions in quartz-bearing pelitic rocks. *Contributions to Mineralogy and Petrology*, 20, 244–267.
- Chakraborty, S. and Ganguly, J. (1992) Cation diffusion in aluminosilicate garnets: Experimental determination in spessartine-almandine diffusion couples, evaluation of effective binary diffusion coefficients, and applications. *Contributions to Mineralogy and Petrology*, 111, 74–86.
- Chernoff, C.B. and Carlson, W.D. (1997) Disequilibrium for Ca during growth of pelitic garnet. *Journal of Metamorphic Geology*, 15, 421–438.
- (1999) Trace-element zoning as a record of chemical disequilibrium during garnet growth. *Geology*, 27, 555–558.
- Christian, J.W. (1975) *The Theory of Transformations in Metals and Alloys: Part I—Equilibrium and General Kinetic Theory*. 586 p. Pergamon Press, Oxford.
- Daniel, C.G. and Spear, F.S. (1998) Three-dimensional patterns of garnet nucleation and growth. *Geology*, 26, 503–506.
- (1999) The clustered nucleation and growth processes of garnet in regional metamorphic rocks from Northwest Connecticut, USA. *Journal of Metamorphic Geology*, 17, 503–520.
- Daniel, C.G., Prior, D., Spear, F.S., Hirsch, D., and Carlson, W. (1999) Testing the model of multiple nucleation sites for complexly zoned garnet; an application of electron backscatter diffraction and orientation contrast imaging. *Geological Society of America Abstracts with Programs*, 31, 168–169.
- Davidow, J.S. (1996) Proterozoic evolution of the Llano Uplift, central Texas: Evidence for high-pressure metamorphism from the Oxford mafic body. M.A. Thesis, University of Texas at Austin, 172 p.
- de Béthune, P., Ladroun, D., and Bocquet, J. (1975) Diffusion processes in resorbed garnets. *Contributions to Mineralogy and Petrology*, 50, 197–204.
- Denison, C. and Carlson, W.D. (1997) Three-dimensional quantitative textural analysis of metamorphic rocks using high-resolution computed X-ray tomography. Part II: Application to natural samples. *Journal of Metamorphic Geology*, 15, 45–57.
- Farver, J.R. and Yund, R.A. (1995a) Grain-boundary diffusion of oxygen, potassium and calcium in natural and hot-pressed feldspar aggregates. *Contributions to Mineralogy and Petrology*, 118, 340–355.
- (1995b) Interphase boundary diffusion of oxygen and potassium in K-feldspar/quartz aggregates. *Geochimica et Cosmochimica Acta*, 59, 3697–3705.
- (1996) Volume and grain boundary diffusion of calcium in natural and hot-pressed calcite aggregates. *Contributions to Mineralogy and Petrology*, 123, 77–91.
- (2000a) Silicon diffusion in a natural quartz aggregate: constraints on solution-transfer diffusion creep. *Tectonophysics*, 325, 193–205.
- (2000b) Silicon diffusion in forsterite aggregates: Implications for diffusion accommodated creep. *Geophysical Research Letters*, 27, 2337–2340.
- Fisher, G.W. (1977) Nonequilibrium thermodynamics in metamorphism. In D.G. Fraser, Ed., *Thermodynamics in Geology*, p. 381–403. D. Reidel Publishing Company.
- Foster, C.T. Jr. (1986) Thermodynamic models of reactions involving garnet in a sillimanite/staurolite schist. *Mineralogical Magazine*, 50, 427–429.
- Ganguly, J., Cheng, W., and Chakraborty, S. (1998) Cation diffusion in aluminosilicate garnets: experimental determination in pyrope-almandine diffusion couples. *Contributions to Mineralogy and Petrology*, 131, 171–180.

- Hirsch, D.M. (2000) Quantitative studies of porphyroblastic textures. Unpub. PhD Dissertation, University of Texas at Austin, 129 p.
- Hirsch, D.M. and Carlson, W.D. (2001) Causes of variation in textures along a regional metamorphic field gradient (abstr.). Eleventh Annual V. M. Goldschmidt Conference, Abstract no. 3203. (CD-ROM).
- Hirsch, D.M., Ketcham, R.A., and Carlson, W.D. (2000) An evaluation of spatial correlation functions in textural analysis of metamorphic rocks. *Geological Materials Research*, 2, 1–21.
- Holdaway, M.J. (2000) Application of new experimental and garnet Margules data to the garnet-biotite thermometer. *American Mineralogist*, 85, 881–892.
- Joesten, R. (1977) Evolution of mineral assemblage zoning in diffusion metasomatism. *Geochimica et Cosmochimica Acta*, 41, 649–670.
- Johnson, C.D. and Carlson, W.D. (1990) The origin of olivine-plagioclase coronas in metagabbros from the Adirondack Mountains, New York. *Journal of Metamorphic Geology*, 8, 697–717.
- Jordan, M.A. (1970) Garnetiferous metagabbro near Babyhead, Llano County, Texas. M.A. Thesis, University of Texas at Austin, 75 p.
- Ketcham, R.A. and Carlson, W.D. (2001) Acquisition, optimization and interpretation of X-ray computed tomographic imagery: applications to the geosciences. *Computers & Geosciences*, 27, 381–400.
- Kretz, R. (1974) Some models for the rate of crystallization of garnet in metamorphic rocks. *Lithos*, 7, 123–131.
- Lang, H.M. and Dunn, G.R. (1990) Sequential porphyroblast growth during deformation in a low-pressure metamorphic terrain, Orrs Island–Harpwell Neck, Maine. *Journal of Metamorphic Geology*, 8, 199–216.
- Lasaga, A.C. (1979) Multicomponent exchange and diffusion in silicates. *Geochimica et Cosmochimica Acta*, 43, 455–469.
- Letargo, C.M.R., Park, J.S., and Lamb, W.M. (1995) Comparison of calcite + dolomite thermometry and carbonate + silicate equilibria: Constraints on the conditions of metamorphism of the Llano uplift, central Texas, U.S.A. *American Mineralogist*, 80, 131–143.
- Misch, P. and Onyeagocha, A.C. (1976) Symplectite breakdown of Ca-rich almandines in upper amphibolite-facies Skagit Gneiss, North Cascades, Washington. *Contributions to Mineralogy and Petrology*, 54, 189–224.
- Mosher, S. (1998) Tectonic evolution of the southern Laurentian Grenville orogenic belt. *Geological Society of America Bulletin*, 110, 1357–1375.
- Rougvie, J.R., Carlson, W.D., Copeland, P., and Connelly, J. (1999) Late thermal evolution of Proterozoic rocks in the northeastern Llano Uplift, central Texas. *Precambrian Research*, 94, 49–72.
- Spear, F.S. and Daniel, C.G. (1998) 3-dimensional imaging of garnet porphyroblast sizes and chemical zoning. Nucleation and growth history in the garnet zone. *Geological Materials Research*, 1, 1–43.
- (2001) Diffusion control of garnet growth, Harpswell Neck, Maine, USA. *Journal of Metamorphic Geology*, 19, 179–195.
- Spear, F.S. and Yao, K. (2001) The 3-dimensional geometry of garnet growth, Harpswell Neck, Maine, USA. Eleventh Annual V. M. Goldschmidt Conference, Abstract no. 3693 (CD-ROM).
- Vance, D. and O’Nions, R.K. (1990) Isotopic chronometry of zoned garnets: growth kinetics and metamorphic histories. *Earth and Planetary Science Letters*, 97, 227–240.
- Whitney, P.R. and McLelland, J.M. (1973) Origin of coronas in metagabbros of the Adirondack Mts., N.Y. *Contributions to Mineralogy and Petrology*, 39, 81–98.
- Wilkerson, A., Carlson, W.D., and Smith, D. (1988) High-pressure metamorphism during the Llano orogeny inferred from Proterozoic eclogite remnants. *Geology*, 16, 391–394.
- Yang, P. and Rivers, T. (2001) Chromium and manganese zoning in pelitic garnet and kyanite: spiral, overprint, and oscillatory zoning patterns and the role of growth rate. *Journal of Metamorphic Geology*, 19, 455–476.
- Zumbro, J.A. (1999) A structural, petrologic, and geochemical investigation of the Valley Spring Gneiss of the southeastern Llano Uplift, central Texas. M.S. Thesis, University of Texas at Austin, 428 p.